Atmos. Chem. Phys. Discuss., 13, 26043–26115, 2013
www.atmos-chem-phys-discuss.net/13/26043/2013/
doi:10.5194/acpd-13-26043-2013

Atmospheric Chemistry and Physics Discussions

Chemical composition and sources of coastal marine aerosol particles during the 2008 VOCALS-REx campaign

Y.-N. Lee[1], S. Springston[1], J. Jayne[2], J. Wang[1], J. Hubbe[3], G. Senum[1], L. Kleinman[1], and P. H. Daum[1]

[1]Atmospheric Sciences Division, Brookhaven National Laboratory, Upton, NY 11973, USA
[2]Aerodyne Research Inc., Bellerica, MA 01821, USA
[3]Pacific Northwest National Laboratory, P. O. Box 999, K8-88, Richland, WA 99352, USA

Received: 3 September 2013 – Accepted: 4 September 2013 – Published: 9 October 2013

Correspondence to: P. H. Daum (phdaum@bnl.gov)

Published by Copernicus Publications on behalf of the European Geosciences Union.

Abstract

The chemical composition of aerosol particles ($D_p \leq 1.5\,\mu m$) was measured over the southeast Pacific ocean during the VOCALS-REx experiment between 16 October and 15 November 2008 using the US DOE G-1 aircraft. The objective of these flights was to gain an understanding of the sources and evolution of these aerosols, and how they interacted with the marine stratus cloud layer that prevails in this region of the globe. Our measurements showed that the marine boundary layer (MBL) aerosol mass was dominated by non-sea-salt SO_4^{2-}, followed by Na^+, Cl^-, Org, NH_4^+, and NO_3^-, in decreasing order of importance; $CH_3SO_3^-$ (MSA), Ca^{2+}, and K^+ rarely exceeded their limits of detection of ~ 0.05 and $\sim 0.15\,\mu g\,m^{-3}$ for anions and cations, respectively. The aerosols were strongly acidic as the NH_4^+ to SO_4^{2-} equivalence ratio was typically < 0.3; this inferred acidity is corroborated by the conductivity of aqueous samples collected by the PILS. Sea-salt aerosol (SSA) particles, represented by NaCl, showed Cl^- deficits caused by both HNO_3 and H_2SO_4, and were externally mixed with SO_4^{2-} particles as the AMS detected no NO_3^- whilst uptake of HNO_3 occurred only on SSA particles. The SSA loading as a function of wind speed agreed with that calculated from published relationships, and contributed only a small fraction of the total accumulation mode particle number. Vertical distribution of MBL SSA particles ($D_p \leq\sim 1.5\,\mu m$) was uniform, suggesting a very limited dilution from entrainment of free tropospheric (FT) air. It was inferred that because all of the aerosol species (except SSA) exhibited a strong land-to-sea gradient, they were of continental origin. Comparison of relative changes in median values using LOWESS fits as proxies suggests that (1) an oceanic source of NH_3 is present between 72° W and 76° W, and (2) additional organic aerosols from biomass burns or biogenic precursors were emitted from coastal regions south of 31° S, with possible cloud processing, and (3) FT contributions to MBL gas and aerosols were negligible. Positive Matrix Factorization analysis of organic aerosol mass spectra obtained with the AMS showed an HOA on 28 October 2008 but not on 6 November 2008 that we attribute to a more extensive cloud processing on the later date. A highly oxi-

ACPD
13, 26043–26115, 2013

dized OOA factor resembling fulvic acid was found associated with anthropogenic and biogenic sources as well as long range transported biomass burn plumes in the FT air. A sulfur-containing OOA factor identified as MSA was strongly correlated with SO_4^{2-}, hence anthropogenic. The very low levels of $CH_3SO_3^-$ observed suggest a limited contribution of DMS to SO_4^{2-} aerosols production during VOCALS.

1 Introduction

To improve understanding of sources and processes governing atmospheric aerosol distributions and aerosol radiative effects through clouds, the southeast Pacific (SEP) region was selected as a study domain by a major international field campaign, the VAMOS[1] Ocean-Cloud-Atmosphere-Land Study-Regional Experiment (VOCALS-REx), organized by National Science Foundation (NSF). The SEP off the coast of Chile and Peru is home to the largest marine stratocumulus cloud deck among those typically found in eastern edges of world oceans, which play an important role in the climate system exerting cooling effects (Wood, Scientific Program Overview, http://www.eol.ucar.edu/projects/vocals/, Wood et al., 2011; Bretherton et al., 2010). This campaign, referred to as VOCALS in this work, was designed to collect observational data to help understand the structure of marine stratocumulus clouds, their radiative properties, and sources of marine aerosol particles that maintain and interact with clouds in the SEP (Wood et al., 2011).

Because aerosol particles serve as cloud droplet precursors and impact cloud microphysical properties, a major effort in VOCALS was focused on characterizing aerosol particles in terms of size distribution, mass concentrations, and chemical composition so that their sources, evolution, and effects on aersol-cloud interactions, could be investigated. In the VOCALS region, the atmospheric system that governs the marine stratocumulus in the SEP is strongly coupled to the ocean and the land whereby the

[1]VAMOS stands for Variability of the American Moonsoon Systems.

ACPD
13, 26043–26115, 2013

Andes mountain range forces the zonal air flow northward along the shore. This highly uniform wind field advects continental emissions from the narrow Chilean coastal regions into the MBL, and intensifies upwelling enhancing productivity with possible increased emission of organic compounds including dimethylsulfide (DMS) (cf., O'Dowd, 2004). Since satellite data showed a strong gradient in effective cloud droplet radius of the marine stratocumulus, smallest near the shore (Wood et al., 2011), implying an increased aerosol number concentration, the sources, most likely anthropogenic, of this increased areosol loading must be identified for an improved understanding of aerosol-cloud interactions and impact of human activities on cloud radiative properties in the SEP region.

Aerosol sources that could impact the MBL of the SEP region include those of continental, marine, and the free troposphere (FT). Several studies of aerosol chemical composition on land and in the MBL during and before VOCALS showed that both SO_4^{2-} aerosol, which dominated aerosol mass, and organic aerosols (OA) were of terrestrial origin, with only small contributions from the ocean and the FT. Tomlinson et al. (2007) identified anthropogenic acidic SO_4^{2-} aerosols during shipboard measurements in the SEP off the coast of Chile and Peru. Chand et al. (2010) identified 4 different types of aerosol sources at Paposo, Chile, several kilometers inland; they include urban/biofuels, soil/smelters, biomass burn, and marine based on Positive Matrix Factorization (PMF) analysis of aerosol components determined from filter samples. Urban/biofuel sources dominated aerosol mass ($\geq 50\,\%$), with marine being the least important at $\leq 15\,\%$. Hawkins et al. (2010) reported shipboard measurements during VOCALS that both SO_4^{2-} and OA were mainly derived from continental outflows. Except for a small marine derived hydroxy-organic class, other aliphatic, carboxyl-organic and organosulfate classes were all of land origin. Yang et al. (2011) showed, based on both shipboard and airborne measurements, that MBL sulfur species (primarily SO_4^{2-}) near the coast were dominated by anthropogenic sources. However, west of 78° W continental influence was minimal and the MBL sulfur is dominated by DMS with minor contributions from entrainment of FT air. Shank et al. (2012), focusing on the identifi-

ACPD
13, 26043–26115, 2013

cation of oceanic OA sources in clean MBL air, found that marine contributions to OA in the SEP was nearly absent because even the very low OA loadings in clean marine air (CO < 61 ppb) were associated with the combustion tracer black carbon. Allen et al. (2011) showed the strong influence of continental emissions to aerosols in the MBL of the SEP east of 80° W, and long range transport of biomass burn plumes rich in OA to the FT in the SEP region. A SO_4^{2-} concentration of 0.3 µg m^{-3} observed in the MBL was considered a background value of the VOCALS region. In this work we report the loadings and chemical composition of fine aerosol particles (D_p < 1.5 µm), measured on board the DOE G-1 in the coastal marine atmospheres off northern Chile using both an Aerosol Mass Spectrometer and a Particle-into-liquid Sampler – Ion Chromatography technique, up to ~ 780 km off shore (77.8° W) between 18.4° S and 20° S. Complementing earlier reports, we examine the sources and evolution of aerosol particles to provide additional characterization of the relative importance of land, ocean, and FT contributions to aerosols that serve as cloud precursors in the coastal MBL of the SEP.

2 Experimental section

The instrumented DOE G-1 aircraft deployed in the VOCALS was supported by the DOE Atmospheric Sciences Program and was among three other aircraft stationed at Arica International Airport, Chile (18°27.44′ S, 70°22.37′ W): NSF C130, UK BAAM Bae-146, and UK NERC Dornier 228 (Wood et al., 2011). The G-1 was equipped with a suite of aerosol and cloud instrumentation for characterizing aerosol chemical composition as well as aerosol and cloud microphysics (Allen, 2011). The study took place over the coastal waters off Northern Chile in the SEP between 15 October and 15 November 2008. The G-1 conducted 17 research flights mainly between 18° S and 20° S, extending west up to ~ 78° W (Fig. 1), typically between 11 a.m. and 3 p.m. local time (LT), each lasting 3–4 h. The date and time of the flights are listed in Table 1.

ACPD
13, 26043–26115, 2013

2.1 Instrumentation

The G-1 was equipped with instruments for characterizing aerosol particles, cloud droplets, trace gas species, atmospheric state parameters and winds (Kleinman et al., 2012). The instruments for determining aerosol chemical composition and size distributions are briefly described below; CO, O_3, and SO_2 instruments are described elsewhere (Springston et al., 2005).

2.1.1 Aerosol mass spectrometer

An Aerodyne Compact Time-of-Flight Aerosol Mass Spectrometer (AMS) was deployed to determine the chemical composition of non-refractory particles in the size range $D_p \sim 70$ nm to 440 nm. In order to maintain a constant transmission efficiency of the particle focusing lens on the AMS within the altitude range of the G-1 during VOCALS (up to ~ 3 km), a constant pressure chamber maintained at 650 mbar was outfitted upstream of the AMS inlet so that the pressure drop across a pinhole into the AMS was independent of flight altitude. The AMS measurement alternated between the mass spectrometer and the particle time-of-flight (pToF) mode of operation, each complete cycle taking ~ 22 s which is the time resolution of the AMS data. The pToF measurements determined the vacuum aerodynamic diameter (D_{VA}) of the particles. The chemical species quantified included NH_4^+, SO_4^{2-}, NO_3^-, Cl^-, and Org (total organics), limits of detection (LOD) being $\sim 0.1\,\mu g\,m^{-3}$ for NO_3^-, Cl^-, and SO_4^{2-}, and $\sim 0.2\,\mu g\,m^{-3}$ for NH_4^+ and Org. A description of the AMS instrument is given by Drewnick et al. (2005).

2.1.2 Particle-into-Liquid Sampler – Ion Chromatography (PILS-IC)

A PILS system (Orsini et al., 2003) was used to determine the bulk chemical composition of particles in the size range $D_p \sim 70$ nm–~ 1.5 µm, the upper size cut being limited by the isokinetic inlet outfitted on the G-1 (see below). The species quantified by

ACPD
13, 26043–26115, 2013

the PILS included Na^+, K^+, Ca^{2+}, Cl^-, NO_3^-, $CH_3SO_3^-$ (MSA), and SO_4^{2-}, with LOD of $\sim 0.3\,\mu g\,m^{-3}$ and $\sim 0.1\,\mu g\,m^{-3}$ for cations and anions, respectively. Time resolution was 180 s, each sample intergrated over a 170 s period. Although lower in time resolution, the PILS complemented the AMS with detection of MSA, a marker product of DMS oxidation (Yin et al., 1990), and refractory materials such as NaCl in SSA particles, all being potentially important in the MBL. In addition to IC analysis, electrical conductivity of the aqueous aerosol samples collected by the PILS was determined at a 10 s time resolution using a conductivity meter (Consort, model C931, Belgium), with an in-line flow-through conductivity cell inserted between the PILS sampler and the IC's.

2.1.3 Isokinetic inlet

The total air flow entering the inlet (sum of that sampled by instruments and the dump flow) was actively controlled using a mass flow controller with real time true air speed, temperature, and pressure as input (Brechtel, 2002). Upon entering the inlet nozzle, the air speed was slowed by a 2-stage diffusion cone wherein the flow was turbulent, resulting in loss of large particles to the wall. At the G-1 cruising speed of $\sim 100\,m\,s^{-1}$, it was estimated that this isokinetic aerosol inlet has an upper size cut of $D_p \sim 1.5\,\mu m$. During in-cloud passages cloud droplets shatter in the diffusion cones resulting in large number of particles (mode $D_p \sim 50\,nm$) that are too small for the AMS and PILS to sample.

2.1.4 Passive Cavity Aerosol Spectrometer Probes (PCASP)

Two PCASP (model 100X, DMT) were used to determine the size distribution of accumulation mode particles (D_p = 0.1 to 3.0 µm) at a 1 s time resolution. One was mounted on a pylon near the aircraft nose; the other inside the cabin, drawing air from the isokinetic inlet sample manifold. The probes were operated with the de-icer heaters on, increasing the sample air temperature by $\sim 20\,^{\circ}C$ over ambient (Haller et al., 2006), resulting in a reduced relative humidity (RH) of $\leq 40\,\%$. During cloud penetrations, par-

ACPD
13, 26043–26115, 2013

tially dried droplets were detected by the outboard PCASP, skewing the size distribution toward larger size particles. Shattered and dried small particles from cloud droplets were detected by the inboard PCASP, skewing the size distribution toward smaller size end. Description of in-cloud measurement artifacts in connection to quantifying cloud interstitial aerosol particles is provided by Kleinman et al. (2012). In-cloud data (liquid water content, LWC > 0.01 gm m^{-3}) are excluded in the present analysis.

2.1.5 Differential mobility analyzer (DMA)

A DMA (Wang, 2003) which draws air from the isokinetic inlet sample manifold was used to determine size distributions of aerosol particles between $D_p \sim 15$ nm and 440 nm. The RH of the sample air was reduced to ∼ 15 % using a Nafion dryer upstream of the DMA. A complete size distribution was determined every 60 s representing an average of two 30 s scans. During cloud penetrations, the DMA also detected small particles resulting from shattered cloud droplets (Kleinman et al., 2012).

2.2 Sampling strategy

The primary objective of the G-1 mission was to characterize the chemical and microphysical properties of aerosol particles and their effects on cloud microphysics. The strategy was to sample below-, in-, and above-cloud so that relations and interactions between aerosol and cloud could be investigated. Because of its limited range (4 h, ∼ 1400 km), the G-1 typically took a straight east-west transect attempting to reach the furthest possible distance from the coast so that a contrast in cloud aerosol relationships could be characterized in both the pristine marine environment off-shore and polluted MBL near the shore. A limitation arising from this strategy was that the below-, in-, and above-cloud segments were not over the same geographical location, but covered adjacent sections in series along the flight track. Because the clouds tended to dissipate westward from land starting around mid-day, the G-1 typically conducted cloud studies during outbound legs when cloud coverage was still extensive, and BL sampling

ACPD
13, 26043–26115, 2013

during the inbound legs when the near-shore clouds had all but dissipated. With this sampling strategy, the G-1 flew west out of Arica into the marine atmosphere and sampled in succession of just below-cloud, in-cloud, and just above-cloud on the outbound leg; on the inbound leg, it typically flew at a constant low altitude of 100 m.

3 Results

3.1 Data coverage

A composite fligth track of all 17 G-1 research flights durng VOCALS is shown in Fig. 1. Except for the 29 October 2008 along-the-shore flight reaching as far south as 23.5° S, the entire G-1 mission was confined between 18.4° S and 20° S. Flight tracks were predominantly east-west to characterize land-sea gradients in aerosol and cloud properties. Regarding altitude, the G-1 spent ∼ 75 %, ∼ 20 %, and ∼ 5 % of its flight below cloud (BC), in cloud, and above cloud (AC), respectively. Cloud base heights during the G-1 study varied between ∼ 750 m and ∼ 1350 m, increasing with distance from the shore.

3.2 Merging AMS and PILS data

The PILS and the AMS both measured aerosol SO_4^{2-}, NH_4^+, and NO_3^-, but only the PILS measured Na^+, Cl^-, and MSA, and only the AMS measured Org. To examine the relationship between all of the species on a common basis, the AMS data are normalized to PILS data using the slope of the least-squares fit of the correlation plot of non-sea-salt SO_4^{2-} (nss-SO_4^{2-}) concentrations determined by these two methods, one for each flight (Table 3), assuming that nss-SO_4^{2-} was present only in particles of $D_p < 440$ nm. Sea-salt SO_4^{2-} (ss-SO_4^{2-}) was calculated using the observed [Na^+] and the sea-water [SO_4^{2-}]/[Na^+] ratio. An example of such a correlation plot is shown for the 28 October 2008 flight (Fig. 2). This normalization adjusts the concentrations of all the

ACPD
13, 26043–26115, 2013

species measured by the AMS by a constant factor, but not their trends and relative concentrations. We note that the comparibility of the AMS and the PILS reflected in the nss-SO_4^{2-} ratios is affected by a number of factors. They include the difference in upper size cuts, the collection efficiency (CE) of the AMS (taken as unity based on the NH_4^+ to SO_4^{2-} ratios, Kleinman et al., 2007; Mathew et al., 2008), the ionization efficiency (IE) of the AMS (Canagaratna, 2007), which showed a sizable variability (Table 3), due likely to an insufficient warm-up time of the AMS (total operation time for each flight was ~ 7 h), and the AMS detects only non-refractory components, excluding SSA particles and the NO_3^- and SO_4^{2-} sequestered therein.

3.3 Aerosol chemical composition

3.3.1 Synopsis

The AMS measured detectable amounts of SO_4^{2-}, NH_4^+, and Org at nearly all locations, but not Cl^- and NO_3^- which were below their LOD's of ~ 0.05 μg m^{-3} throughout the study. NaCl in SSA particles which are refractory is not detected by the AMS under our operating conditions. NO_3^- was not detected by the AMS because it was present as the refractory $NaNO_3$ in SSA (see below). The PILS detected Na^+, Cl^-, NO_3^-, as well as NH_4^+ and SO_4^{2-}; MSA was found in only a few samples, and K^+ and Ca^{2+} were near their LOD's of ~ 0.15 μg m^{-3} throughout. Chemical composition of MBL aerosol particles was dominated by SO_4^{2-}, which on average accounted for ~ 50 % of the measured total aerosol mass, followed by Na^+, Cl^-, Org, NO_3^-, and NH_4^+, each with a contribution of < 15 %. A strong land-to-sea gradient was seen in NH_4^+, SO_4^{2-}, Org, and NO_3^-, while Na^+ and Cl^- were fairly uniformly distributed longitudinally. These aerosol composition characteristics were fairly consistent during the month long study, and are well represented by the data collected on the 28 October 2008 flight which is described below.

ACPD
13, 26043–26115, 2013

3.3.2 28 October 2008 flight

The G-1 flew west along 18.5° S after taking off at 9.58 a.m. LT and repeated a below-, in-, and above-cloud staircase pattern until reaching the westernmost point (77.8° W, Fig. 3a). The BC transects during the outbound segment were at ~ 600 m. After turning around and headed to Arica, the G-1 sampled MBL air at 100 m until making an approach for landing. The BC NH_4^+, SO_4^{2-}, Org, and NO_3^- concentrations which showed a clear land-to-sea gradient, were nearly invariant at a given location during the 4 h flight period, the values at 600 m (outbound) and at 100 m (inbound) being identical to within 10 % (Fig. 3b and c). In contrast, concentrations of Na^+ and Cl^-, representing SSA particles, were rather constant longitudinally; the Cl^- deficit, caused by uptake of gas phase HNO_3 and in-cloud H_2SO_4 production, was more pronounced near the shore (Fig. 3d). Concentrations of all aerosol species dropped significantly during in-cloud segments (colored sections of the altitude trace in Fig. 3a) because aerosol particles turned cloud droplets were not detected by the AMS and the PILS. The AC air also showed much lower concentrations of most of the species than observed in BC, reflecting a generally cleaner conditions of the FT whose air masses are typically derived from long range transport, thereby more aged and had undergone cloud processing by which soluble substances had been removed (Kleinman et al., 2012).

3.4 Ensemble aerosol chemical composition

The clear air aerosol chemical composition determined for the entire mission is examined in this section to allow composite horizontal and vertical distribution patterns to be characterized. The data are segregated into the BC (RH > 50 % and LWC < 0.01 g m^{-3}) and AC (RH < 45 % and LWC < 0.01 g m^{-3}) regions. We point out that some of the samples identified as AC, in particular those near the shore, had no clouds below them, but are assigned as FT based on potential temperature data. Some AC data were below the inversion, devoid of clouds but remained moist. In this work, AC is interchangeably used with FT.

ACPD
13, 26043–26115, 2013

3.4.1 Composite longitudinal distributions

Concentrations of BC SO_4^{2-}, NH_4^+, and Org determined using the AMS and Na^+ and NO_3^- determined using the PILS are plotted as a function of longitude in Fig. 4. Overlaid on the data points are box plots of one-degree binned data in longitude for SO_4^{2-}, NH_4^+, and Org, and two-degree binned data (separated by −72, −74, and −76° W) for Na^+ and NO_3^-. AC concentrations of these 5 species are plotted analogously, but with RH shown to identify recent surface contacts (Fig. 5). All the box plots in this work show the median and the inner quartiles by the center, bottom, and top cross bars of the rectangular boxes, and the 5 % and 95 % ranges by the wiskers.

Although box plots are commonly used to summarize data patterns with centers and spreads, they are stepwise because of binning. In order to present data patterns in a continuous fashion to facilitate comparisons, we utilize the Locally Weighted Scatter Smoothing lines, LOWESS (Cleveland, 1979), to supplement the box plot approach. Being insensitive to outliers, LOWESS fits closely approximate median values, and deviate only when data density significantly drops. The suitability of this approach is demonstrated in Figs. 4 and 5 where the LOWESS fits agree well with the median values defined by the boxplots except for the westernmost bins where they diverge slightly.

The LOWESS fits, as proxy for medians, exhibit pronounced land-to-sea gradients in the BC concentrations of SO_4^{2-}, NH_4^+, Org, and NO_3^- (Fig. 4). In contrast, the median of Na^+, representing SSA, exhibited a rather uniform longitudinal distribution, increasing slightly offshore. These gradients are consistent with a continental source for SO_4^{2-}, NH_4^+, Org, and NO_3^-. The median AC concentrations of SO_4^{2-} and NH_4^+ (Fig. 5) also exhibited a land-to-sea gradient, showing the influence of nearby terrestrial sources, likely in Chile and Peru (Allen et al., 2011). Higher AC concentrations of SO_4^{2-}, NH_4^+, as well as Org, near the shore (east of ∼ 73° W) were associated with moist air (RH up to ∼ 50 %, Fig. 5) that was likely transported vertically from surface by diurnal pumping in the steep coastal terrain followed by advection to the Pacific (Bretherton et al., 2010;

ACPD
13, 26043–26115, 2013

Allen et al., 2011; Kleinman et al., 2012). Unlike SO_4^{2-} and NH_4^+, the median AC Org concentration exhibited almost no longitudinal dependence, with only a slight dip at the westernmost reach of the G-1, indicating long range transport of air masses enriched in Org but depleted in SO_4^{2-} and NH_4^+ had impacted the FT west of 73° W. We note that while the driest AC air typically contained the lowest SO_4^{2-} and NH_4^+ (in red, Fig. 5), the AC Org was still appreciable in the driest air derived from long range transport appearing between ~ 74° W and ~ 76° W. This observation suggests that OA, presumably associated with biomass burns (Allen et al., 2011), was not completely removed by wet processes which were inferred from low [Org]/[CO] ratios (Kleinman et al., 2012).

AC concentrations of Na^+ were much smaller than that of BC (Fig. 5), but nonetheless showed a small gradient higher near the coast associated with moist air pumped to the FT. Only a few AC samples contained measurable NO_3^-. Due to the limited number of AC data points, no box plots were made for these two species, and no LOWESS for AC NO_3^-. The number of PILS samples in the FT was small because not only the G-1 had spent a very limited amount of time above cloud (~ 5 %), but also because only a small fraction of AC PILS samples were free of cloud contamination due to their long 3 min sampling time period.

Aerosol MSA, a product of DMS from OH addition reaction favored at lower temperatures (e.g., Yin et al., 1990), was all but absent; only 50 out of the 1150 PILS samples had concentrations greater than its LOD of 0.05 µg m^{-3}; only 15 were greater than 0.1 µg m^{-3} (Fig. 6). All 50 samples were close to the shore, i.e., east of 72.5° W.

3.4.2 Composite vertical distributions

The altitude dependence of BC and AC concentrations of SO_4^{2-}, NH_4^+, and Org determined by the AMS are shown in Fig. 7. We note BC and AC data overlapped between ~ 800 m and ~ 1500 m, reflecting the variability in local BL height and cloud thickness, as well as a systematic increase of MBL height off shore (Rahn and Garreaud, 2010). The LOWESS fits show BC [SO_4^{2-}] was significantly higher than that of AC, and a clear

ACPD
13, 26043–26115, 2013

discontinuity exists between BL and FT. This BC-AC difference is less distinct for NH_4^+ and nearly absent for Org (Fig. 7). The LOWESS fit of BC SO_4^{2-} determined by the PILS showed a vertical pattern in good agreement with that for the AMS data (Fig. 7). The median BC concentration profiles also show apparent maxima at altitudes of ∼ 450 m, ∼ 250 m, and ∼ 500 m for SO_4^{2-}, NH_4^+, and Org, respectively (Fig. 7). Finally, we note that while the BC $[Na^+]$ exhibited a small vertical gradient, decreasing with altitude, BC $[NO_3^-]$ which was found to reside on SSA particles showed a vertical profile similar to those of SO_4^{2-} and Org, and a maximum at ∼ 350 m (Fig. 8). We point out that these composite distribution patterns are influenced by sampling biases with respect to time and location, and do not represent true vertical variability of a quantity at a given location and time like a sounding. Kleinman et al. (2012, Fig. 5) showed that the G-1 sampled closer to the shore (where concentrations were higher) at ∼ 500 m (median longitudes at ∼ 71.5° W) than other altitudes (median longitude ∼ 73° W, where concentrations were lower). Even with this idiosyncrasy, we nonetheless expect to gain useful insights, in a statistical sense, into sources, chemistry, and transport of the simultaneously measured chemical species by comparing their relative changes in the distributions.

4 Discussion

4.1 Comparison of concentrations of aerosol mass with aerosol volume

To examine the quantitativeness of the aerosol mass concentration measurements, we compare the total aerosol mass concentrations to the total aerosol volume concentrations calculated from size distributions determined by the DMA. Because the AMS and the DMA cover the same particle size range, these ratios should approximate the particle density if the DMA measured dry particles and if all aerosol components were determined. For the 28 October 2008 flight, the total mass concentration (the sum of all of the ionic species identified by the PILS and the Org identified by the AMS) shows

ACPD
13, 26043–26115, 2013

a good linear relationship with the total DMA volume (Fig. 9a). However, because the PILS also detected particles between $D_p \sim 0.44\,\mu m$ and $\sim 1.5\,\mu m$ which are presumably due mainly to SSA, we also compare the nss fraction of the PILS mass concentrations (by excluding Na^+, Cl^-, Mg^{2+}, ss-SO_4^{2-}, and NO_3^-) to the DMA volume (Fig. 9a). Because the correlation between nss aerosol concentrations with the DMA volumes further improved, the supposition SSA particles were mainly of size $D_p \geq 440\,nm$ appears justified. We point out that the pToF measurements show that the average D_{va} of SO_4^{2-} particles in the MBL on 28 October 2008 was 455 nm, corresponding to a D_g of $\sim 280\,nm$ using a density of $\sim 1.7\,g\,cm^{-3}$. The sizes of the NH_4^+ and Org particles could not be determined because of their low concentrations.

The near unity slope (Fig. 9a) is smaller than the density of SO_4^{2-} aerosols of $\sim 1.7\,g\,cm^{-3}$. Two possible reasons are: first, there might be undetected components by the PILS, including non-activated particles and unquantified ionic species. Regarding the latter, we note that the observed conductivity of the aqueous PILS samples were at times greater than that calculated from the identified species, supporting this possibility (see below). However, we recognize that any organic ionic species may not contribute to the mass differences as they were accounted for by the AMS. Second, the DMA volume may be overestimated as it could include the water asscociated with the un-nuetralized H_2SO_4 at the DMA's operating RH of $15 \pm 2\,\%$. Kleinman et al. (2012) showed that a solution containing NH_4HSO_4 and H_2SO_4 mixed with 10 % insoluble organics similar to the aerosol composition observed during VOCALS is calculated to exhibit a volume growth factor of 1.3 at RH = 15 %. With this growth factor taken into account, there is a $\sim 25\,\%$ underestimation of aerosol mass compared to the DMA volume, part of it could be casued by unidentified constituents. The total AMS mass concentration also strongly correlated with the total DMA volume concentration (e.g., 28 October 2008, Fig, 9b). Again, taking into consideration of the H_2O in the DMA volume, the AMS mass concentrations were underestimated by $\sim 30\,\%$, suggesting a possible over correction (cf. normalization factor = 1.54) provided there were no other aerosol species contributing to the DMA volume.

ACPD
13, 26043–26115, 2013

4.2 Aerosol acidity

The aerosol composition determined on the G-1 was dominated by SO_4^{2-}, with NH_4^+ and Org each accounting for no more than 15 % of the total mass. The median values of BC NH_4^+ to SO_4^{2-} equivalence ratios as a function of longitude varied from 0.25 to 0.3 (Fig. 10), indicating the SO_4^{2-} aerosols were only partially neutralized and strongly acidic. As shown by the whiskers, > 90 % of the samples were acidic as their NH_4^+ to SO_4^{2-} equivalence ratios were ≤ 0.8. This ratio is examined in terms of charge balance of the ionic species using data of 28 October 2008 as an example to identify the reason why it is so low. A plot of the total positive charges against the total negative charges shows an overwhelming cation deficit as all the data points lie below the 1 : 1 line of charge neutrality (Fig. 11). By assuming that the missing cations are associated with nss-SO_4^{2-}, we recalculated the total positive charges by adding that associated with nss-SO_4^{2-} and subtracting NH_4^+; the new plot shows a nearly perfect charge balance (Fig. 12), confirming that the missing cations are associated with nss-SO_4^{2-}. However, since charge neutality in itself does not identify the missing cation(s), we use conductivity of the PILS samples to provide evidence that H_3O^+ was the plausible missing cation.

The time series of the conductivity of PILS samples on 28 October 2008 is shown along with that calculated from the ions measured by the PILS (in red and green traces, respectively, Fig. 13). The calculated conductivity includes H^+ and HCO_3^- in equilibrium with atmospheric CO_2 (380 ppm, Henry's low solubility $H_{CO_2} = 0.04\,M\,atm^{-1}$, dissociation constant $K_a = 4.25 \times 10^{-7}$ M, both at 25 °C) assuming the pH of the liquid sample was governed by CO_2. Although the trends are identical, the calculated conductivity is significantly smaller than the observed, except during the in-cloud and above-cloud segments where the aerosol loading was greatly reduced. We point out that a positive offset of $0.15\,\mu S\,cm^{-1}$ was added to the calculated so that the lowest conductance matches that of the observed in the FT (15:00–15:10, Fig. 13) where a minimum

ACPD
13, 26043–26115, 2013

aerosol loading is expected. With the assumption that H_3O^+ is the missing cation, the recalculated conductivity (blue trace, Fig. 13) shows a much improved agreement with the observed with > 80 % of the differences accounted for. Because no other cations can make up this difference due to their much smaller equivalent conductances compared to that of the H_3O^+, we conclude that H_3O^+ was indeed the missing cation. The conclusion that the SO_4^{2-} aerosols were strongly acidic agrees with Tomlinson et al. (2007) based on aerosol volatility properties. We note that the calculated conductance was lower than the observed in the BL between ∼ 73° W and ∼ 77° W with a magnitude upward of 0.1 µS cm^{-1}. This discrepancy suggests the presence of other ionic species that were collected but not identified by the IC. Similarly, the calculated conductivity was lower than the observed during the first three AC transects near the shore but not during the last three off shore, suggesting the presence of appreciable aerosol loading in the AC layer whose ionic components were not identified (e.g., dust and OA). This elevated AC serosol loading is corroborated by the much higher RH in the first three AC transects (∼ 20 %) than the last three (< 5 %).

4.3 Sea-salt aerosol characterization

While the main production mechanism of SSA particles is bubble bursting followed by wave breaking which is strongly WS dependent, the SSA loadings in MBL are governed by a number of factors, including production, entrainment, transport, mixing height, as well as removal by precipitation and dry deposition (Lewis and Schwartz, 2004). The observed SSA concentrations during VOCALS represent an ideal data set to be compared with the established relationship between loading and WS because of the expansive and uniform wind field characterizing the SEP (Rahn and Garreaud, 2010).

4.3.1 Wind speed dependence of SSA loading

The WD in the MBL measured on the G-1 showed a bimodal distribution with peaks at ∼ 160° and ∼ 190° (directions the wind was from), with only a single mode at ∼ 160°

ACPD
13, 26043–26115, 2013

west of 71.5° W (Fig. 14a). This wind pattern, i.e., southerly near the shore and south-southeasterly off-shore, supports the pattern calculated by Rahn and Garreaud (2010). The MBL WS measured on the G-1 is plotted as a function of longitude in Fig. 14b; the LOWESS fit of WS increased with distance off-shore from $\sim 3.5\,m\,s^{-1}$ to $8\,m\,s^{-1}$. but showed no altitude stratification (Fig. 14b). Because the wind-stress induced SSA production is thought to take effect at WS $>\sim 5\,m\,s^{-1}$, we calculated the SSA concentration increase to be a factor of 1.8 from $6\,m\,s^{-1}$ to $8\,m\,s^{-1}$ based on the canonical size distribution given by Lewis and Schwartz (2004). The observed increase of the median $[Na^+]$ from ~ 75° W to ~ 78° W (Fig. 4), corresponding to the same WS increase, is only ~ 1.3, but is adjusted to ~ 1.5 with the deepening of the MBL from ~ 1.2 km to ~ 1.4 km taken into account, still smaller than the factor of 1.8 predicted. We note that because the SSA concentrations discussed here are based on particles of $D_p \leq 1$–2 µm, whose atmospheric life times are sufficiently long that their concentrations in the uniform wind field of SEP have approached a steady state, they are less sensitive to local WS than SSA particles of $D_p > 2$ µm which were not sampled.

The LOWESS fit of the WS dependence of BC [NaCl] (Fig. 15) shows a positive correlation between the two quantities for WS $\geq 6\,m\,s^{-1}$ consistent with the notion of a threshold WS for wind stress induced SSA production. This observed WS dependence of [NaCl] is nearly parallel to that recommended by Lewis and Schwartz (2004, Fig. 17 therein), scaled to reflect NaCl (blue line, Fig. 15). Since the isokinetic inlet on the G-1 is thought to effect an upper size cut of $D_p \sim 1$ to 2 µm, we evaluate the NaCl loadings according to these two size limits based on the canonical size distribution at WS's of 7 and $9\,m\,s^{-1}$ (Lewis and Schwartz, 2004, Table 14) for comparison (Fig. 15). The observed median values are flanked by these calculated values, but are closer to that for a 1 µm size cut than a 2 µm. In view of the large uncertainty of $x \div 3$ of the canonical values of WS dependent SSA loading (Lewis and Schwartz, 2004), this agreement supports, albeit loosely, the upper size cut of the isokinetic inlet on the G-1. We point out that the particle size used in the calculations were for SSA in equilibrium

ACPD
13, 26043–26115, 2013

at RH = 80 %, and the observed median BC RH values increased from ~ 70 % near the sea surface to ~ 90 % just below the cloud.

The total SSA number concentration, N_{SSA}, estimated from the canonical size distribution are 3.5 cm^{-3} and 6.0 cm^{-3} at WS = 7 $m\,s^{-1}$ and 9 $m\,s^{-1}$, respectively, which exceeded the total N_{SSA} under D_p = 2 µm by only ~ 5 %. Consequently, in terms of number concentration, the SSA represented only a tiny fraction of the total accumulation mode particles even over the cleanest region the G-1 surveyed which was ~ 150 cm^{-3}.

For WS ≤ 6 $m\,s^{-1}$, there was a small negative WS dependence of [NaCl] (Fig. 15). Since bubble bursting associated with wave breaking is no longer the main source of SSA in this WS range, the elevated SSA levels observed are either transported from upwind or produced from different mechanisms. Recognizing that the near-shore WS was the lowest (Fig. 14b), we surmise that wave breaking in coastal surf zone was an important source of SSA which diminishes with distance from the shore and manifested in the observed negative WS dependence. Futher, because of the southerly along the north-south oriented shoreline, substantial levels of SSA can result due to accumulation effect. From our observations, surf zone production can have a signicant impact on SSA loading up to ~ 74° W, some ~ 400 km away from the coast.

The composite WS dependence of SSA concentrations discussed above is well represented by the data of 28 October 2008 flight which clearly demonstrated the importance of surf generated SSA in near-shore/low-WS conditions. First, we note that the BC WS increased from ~ 3 $m\,s^{-1}$ to ~ 10 $m\,s^{-1}$ with distance from the shore, which remained unchanged over the course of the flight as the outbound and inbound data essentially coincided (Fig. 16). However, [Na^+] remained nearly constant at ~ 0.30 µg m^{-3} (inbound, ~ 100 m) and ~ 0.20 µg m^{-3} (outbound, ~ 600 m) (Fig. 16), the difference being discussed later. The observed [NaCl] at the lower altitude, ~ 0.8 µg m^{-3}, agreed well with literature values evaluated for an upper size cut of 1 µm, i.e., ~ 0.7 ($x/\div 3$) µg m^{-3} at WS = 7 $m\,s^{-1}$ (Fig. 15). Although at a first glance the SSA concentrations seemed rather constant across 70.5° W to 77.5° W where WS increased from 3 $m\,s^{-1}$ to 10 $m\,s^{-1}$ (Fig. 16), a closer inspection revealed a clear correspondence between [Na^+] and WS

ACPD
13, 26043–26115, 2013

above $\sim 7\,m\,s^{-1}$ (west of $\sim 74^{\circ}$ W). We attribute the elevated SSA loading near the coast (east of $\sim 74^{\circ}$ W) to surf zone SSA production which masked the trend of wind induced SSA concentrations. To a lesser extent, the WS dependent SSA increase toward the open ocean was attenuated by a deepening of MBL height. The observed MBL height on 28 October 2008 increased from ~ 1250 m to ~ 1450 m across shore, resulting in a ~ 10 % attenuation.

4.3.2 Size dependence of SSA on RH

The different BC SSA concentrations at two different heights, i.e., $[Na^+] \sim 0.30\,\mu g\,m^{-3}$ at ~ 100 m and $\sim 0.2\,\mu g\,m^{-3}$ at ~ 600 m, seem to suggest a vertical graident in SSA (Fig. 16), although no such a vertical gradient was observed in $[SO_4^{2-}]$. While SSA particles may manifest an overall vertical gradient due to their larger sizes and sea surface origin, a vertical gradient for particles with $D_p < 1.5\,\mu m$ is unlikely due to their relatively long atmospheric times. This is true if an air mass is continuously exposed to SSA input for a duration significantly longer than the characteristic vertical mixing time (t_m) as the life times against loss mechanisms, including gravitational settling, dry deposition, and coagulation, are all fairly long (Slinn, 1983). For an estimated $t_m \leq 1$ h, an 8 h travel time (~ 250 km at a WS of $\sim 8\,m\,s^{-1}$) is sufficient to result in a uniform vertical distribution for particles with $D_p \leq 2\,\mu m$. Without a vertical gradient, the observed difference in $[Na^+]$ at the two different heights is believed to be caused by a size dependence of SSA on RH (Tang et al., 1997) discriminated by the upper size cut of the isokinetic inlet. Particles grow larger at 600 m (RH ~ 82–92 %) compared to 100 m (RH ~ 68–78 %), which reduces the upper size cut at the higher altitude by a ratio of r_{87}/r_{73} of ~ 1.3, e.g., 1.2 µm vs 1.5 µm which correspond to dry sizes of ~ 0.6 µm and ~ 0.8 µm, respectively.

To seek additional evidence for this RH effect on SSA size, we compare the accumulation mode particle number concentrations between $D_p = 0.5\,\mu m$ and 3 µm ($N_{0.5-3}$) determined at the two different altitudes by the inboard PCASP, expecting a smaller concentration at the higher altitude. These sizes are associated with SSA particles as

ACPD
13, 26043–26115, 2013

it has been shown that SO_4^{2-} particles are much smaller. The validity of this comparison however requires (1) the PCASP measurement be unaffected by ambient RH, which we assume to be the case for clear air aerosols, and (2) the aerosol loadings at a given location where the two altitudes were sampled remained unchanged over the G-1 flight. Regarding the latter, we note that neither the total DMA volume nor $[SO_4^{2-}]$ changed between the two altitudes for all locations. LOWESS fits of $N_{0.5–3}$ (60 s-smoothed 1 s data) for the 28 October 2008 flight were ~ 25 % lower at 600 m than that at 100 m for the three off shore locations consistent with the observed $[Na^+]$ differentials (Fig. 17). However, despite a similar $[Na^+]$ differences at the two near-shore locations, $N_{0.5–3}$ were comparable at the two altitudes. It is conceivable that unidentified large aerosol particles such as dust may contribute in this size range near the shore, which could also be responsible for the increased conductivity discussed earlier. In fact, we note $[Na^+]$ tracked well with the LOWESS fit of $N_{0.5–3}$ throughout the low altitude transect (Fig. 17), lending support to the presumed size range of the SSA particles.

To further test the effect of RH on the upper size cut of SSA, we examine the $N_{0.5–3}$ measured with the outboard PCASP which sampled aerosols directly from ambient air without a formal inlet. For the 100 m altitude transect, the LOWESS fit of $N_{0.5–3}$ (Fig. 17, 1 s data points not shown) is seen to follow a nearly identical trend as that of $N_{0.5–3}$ determined by the inboard PCASP but showed a greater magnitude by ~ 60 %. The 600 m altidude transect showed LOWESS fit values (broken blue thin line) either comparable or higher than the low altitude values, suggesting that particles grown to larger sizes at higher RH were also detected. For the westernmost points, we note that there was a change in longitude in the two altitudes, which may be responsible for the observed difference in $N_{0.5–3}$.

4.4 Uptake of HNO_3, H_2SO_4 and CH_3SO_3H by SSA particles

SSA particles often exhibit Cl^- deficit caused by strong acids, H_2SO_4 and/or HNO_3, which drive off the volatile HCl, leaving behind the respective Na salts (e.g., Kawakami

ACPD
13, 26043–26115, 2013

et al., 2008). The Cl^- deficit observed during VOCALS was substantial, showing a mission-averaged Cl^- to Na^+ molar ratio of 0.77, representing a loss of ~1/3 of Cl^- (Fig. 18). With NO_3^- detected by the PILS, HNO_3 is identified as an acidifying reagent contributing to the observed Cl^- deficit. In contrast, the AMS detected no NO_3^- (LOD of ~ 0.1 μg m^{-3}) throughout the entire mission. This divergent observation is consistent with not only that the AMS is oblivious of the refractory $NaNO_3$ on SSA, but also that no HNO_3 uptake occurred on the acidic SO_4^{2-} aerosols. These observations in combination with their variant production mechanisms, show that SSA and SO_4^{2-} aerosols remained externally mixed in the MBL. In this regard, we note that MSA, if present, would behave similarly to HNO_3, i.e., retained as a Na salt in SSA but not in the acidic SO_4^{2-} aerosols and therefore not detected by the AMS. HNO_3 is presumably derived from NO_x emitted from combustion sources that are also responsible for SO_4^{2-} and precursors, with a time constant of oxidation of NO_x to HNO_3 being ~ 1 day at [OH] ~ 4×10^6 cm^{-3}. We note that gas phase SO_2 oxidation to H_2SO_4 by OH has a similar rate, being ~ 1–2 % h^{-1}. The uptake of highly soluble gases such as HNO_3 by SSA is governed by gas phase diffusion, with a time constant proportional to SSA radius and concentration (Lewis and Schwartz, 2004). For the SSA size distrbution at WS = 6 m s^{-1}, we estimate an R ~ 1.1 μm cm^{-3} (for $R_p \leq 2$ μm) and a characteristic uptake time of ~ 2 h (and shorter, with the presence of SSA having $R_p > 2$ μm). On the other hand, dry deposition to ocean surface is a potentially important loss mechanism for the highly soluble HNO_3 and is estimated to exhibit a characteristic time of ~ 7 h using a dry deposition velocity of 4 cm s^{-1} and a reference height of 1 km. The removal by washout process during precipitation events is episodic and is expected to be less important than the first two mechanisms described above. The slow NO_x oxidation process allows a characteristic transport distance of NO_x of ~ 500 km at WS = 6 m s^{-1}. With these rates, HNO_3 is essentially removed by SSA without delay after formation. Despite a relatively long NO_x lifetime, it is interesting to note that ~ 37 % of PILS samples showed levels of NO_3^- below its LOD (i.e., ~ 0.05 μg m^{-3}), but none for SO_4^{2-}. While

ACPD
13, 26043–26115, 2013

we can attribute the loss of SSA-bound NO_3^- to preferential removal of SSA particles through drizzle because of their larger sizes (Twohey et al., 2012), we note that the SSA loadings in samples where $[NO_3^-] = 0$ were only a factor of ~ 2 lower than those with $[NO_3^-] > 0$. This suggests SSA particles, at least those with $D_p \leq \sim 2\,\mu m$, are rapidly replenished after precipitation events.

The observed aerosol NO_3^- concentrations only explained a portion of the Cl^- deficit: with NO_3^- taken into account, a $\sim 25\,\%$ Cl^- deficit remains, presumably due to H_2SO_4. Incorporating H_2SO_4 into SSA can in principle be achieved by uptaking of gaseous H_2SO_4, coagulation with sulfate aerosols, and in-cloud oxidation of SO_2. The rate of collision coalescence of SSA with sulfate aerosols is too slow to be important for acidifying SSA. The characteristic time constant for removing SO_4^{2-} particles at SSA particle concentration of $\sim 4\,cm^{-3}$ and a coalescence coefficient of $K \leq 5 \times 10^{-9}\,cm^3\,s^{-1}$ is estimated to be ≥ 500 days. Although in-cloud aqueous oxidation process can in principle be important considering its fast reaction kinetics and the prevalence of cloud in the study region, a quantitative evaluation is unfortunately untenable because the key oxidant H_2O_2 was not determined and the concentration of SO_2 was always below the LOD of our instrument of 0.2 ppb.

4.5 Composite longitudinal distributions of aerosol and gas constituents

The composite longitudinal distributions of SO_4^{2-}, NH_4^+, and Org taken as their LOWESS fits normalized to their maximum concentrations at the easternmost location (see, e.g., Fig. 5) are shown in Fig. 19a. These median concentrations decreased steeply with distance from land indicating their continental origins. The longitudinal gradients observed in a narrow latitude band ($\sim 19^\circ$ S) reflects medians of the remaining concentrations of continental emissions advected into the MBL. According to back trajectory calculations by Allen et al. (2011, Fig. 4), continental emissions received along the 20° S parallel from the coast to the open ocean originated from the Chilean coast moving progressively southward. The 5 day back trajectories originating from

ACPD
13, 26043–26115, 2013

20° S show that for 72° W and 76° W, land contact occurred at around 26° S–30° S and 30° S–40° S, respetively. However, since the back trajectories also show that because of the wind speed gradient, higher off shore, the ages of the air masses sampled along the 19° S parallel since land contact were roughly comparable (~ 3–4 days). Consequently we surmise that the emissions had been aged and processed when sampled, and the longitudinal concentration gradients were due mainly to a higher degree of dilution with higher wind speed off shore. This dilution characteristics is roughly approximated by the normalized longitudinal distribution of the conservative tracer CO (Fig. 19a) provided the CO emission factor remained relatively invariant, and that an appropriate background value can be assigned. Regarding the latter, we chose 62 ppb, the average of the lowest 5 % [CO], which is similar to the 61 ppb used by Shank et al. (2012). Since background air can have different levels of CO depending on its history, choosing a single value to estimate the excess CO ($[CO]_{ex}$) has a relatively large uncertainty for regions of fairly low total [CO]. Finally, the fact that the highest $[CO]_{ex}$ near the shore was only ~ 14 ppb indicates that a significant dilution had occurred to the emissions from the sources considering a typical urban $[CO]_{ex}$ of ~ 200 ppb and greater.

Atmospheric concentration of a trace species decreases with dilution and removal, and increases with additional emissions and/or production. In the VOCALS study domain, the factors governing aerosol/trace gas evolution in the MBL may be simplified because of a uniform wind field, somewhat homogenized (by the southerlies along the coast) regional urban and industrial emission characteristics, and the lack of appreciable oceanic sources. Large point sources such as smelters located typically at higher altitudes along the Chilean caldera were found to contribute minimally to MBL aerosol loadings during VOCALS (Twohy et al., 2012). However, in principle, one emission that may manisfest a varied longitudinal impact along 19° S parallel is continental biogenic emissions which are potentially important only from south of ~ 31° S, as the arid Atacama desert lying north is devoid of any significant biological activity. Consequently, the near shore segments of the G-1 flights along ~ 19° S received nearby continental emissions (e.g., urban, industry, and dust) with little biogenic contributions, but the

ACPD
13, 26043–26115, 2013

offshore segments may receive biogenic aerosols and their precursors from coastal regions further south. Removal of accumulation mode size particles is dominated by wet deposition of rain out and wash out, and dry deposition is playing only a small role (Slinn, 1983). Production of SO_4^{2-} is expected to result from in-cloud oxidation of SO_2 by O_3 and H_2O_2. Production rate by O_3 between 74° W and 78° W can be estimated from the observed medians $[O_3] \sim 30$ ppb, $[SO_2] \sim 25$ ppt (Yang et al., 2011a; Saide et al., 2012), LWC $\sim 0.2\,g\,m^{-3}$, and pH ~ 5: $\sim 0.02\,\mu g\,m^{-3}\,day^{-1}$ assuming clouds occupy ~ 20 % of a 1 km deep MBL. This median SO_4^{2-} production rate due to O_3 (at 30 ppb) is slower than that due to H_2O_2 (at 1 ppb) by ~ 20 fold, and slower still for regions east of 74° W because of a higher cloud water acidity for which the O_3 pathway slows down further. Although gas phase concentration of H_2O_2 was not measured, Benedict et al. (2012) reported a mean cloud water $[H_2O_2] \sim 130\,\mu M$, corresponding to a gas phase H_2O_2 of ~ 1 ppb. Consequently within the G-1 domain, in-cloud SO_2 oxidation is dominated by the H_2O_2 pathway if $[H_2O_2] \sim 1$ ppb attains, which would result an SO_2 oxiation rate of $\sim 150\,\%\,h^{-1}$ at a LWC $\sim 0.2\,g\,m^{-3}$ (Schwartz, 1984). In contrast, gas phase oxidation of SO_2 by the OH radicals is much slower, i.e., $\sim 1\,\%\,h^{-1}$ at a [OH] $\sim 4 \times 10^6\,cm^{-3}$ evaluated for the VOCALS domain by Yang et al. (2011). Entrainment of FT air leads to dilution unless a given species is enriched in the FT compared to the MBL.

The normalized longitudinal distributions of aerosol SO_4^{2-}, NH_4^+, NO_3^-, and Org median concentrations (Fig. 19a) that are adjusted for dilution based on CO distribution (Fig. 19b) all decreased with distance from the shore, but at different rates. Because the air masses were considered well aged, the concentrations observed represented that of the end products that had undergone removal and dilution. Regarding sulfur compounds, we note that the median $[SO_4^{2-}]$ nearest the land was $2.5\,\mu g\,m^{-3}$ (Fig. 4), corresponding to a $[SO_2] = 0.63$ ppb. The mean gase phase $[SO_2]$ reported by Yang et al. (2011) for the same longitude (at 20 S) is 75 ppt, indicating that SO_4^{2-} production was near complete, accounting for ~ 90 % of the sulfur. An emission factor $[S_T]/[CO]$ is estimated to be ~ 0.705/14 = 0.05 ($S_T = SO_2 + SO_4^{2-}$), which is conisdered a minimum

ACPD
13, 26043–26115, 2013

value as possible SO_4^{2-} loss had already occurred when the air masses were sampled at ~ 70.4° W. At the westernmost point, we assume $S_T = SO_4^{2-}$ as the processing time was sufficiently long (> 4 days according to back trajectory calculations) that all sulfur from land emissions was oxidized. With a $[CO]_{ex} \sim 5.8$ ppb, S_T at the source was ~ 0.29 ppb, or a $[SO_4^{2-}] \sim 1.2\,\mu g\,m^{-3}$. Since the observed was only ~ 0.35 $\mu g\,m^{-3}$, ~ 70 % of sulfur had been removed when the air mass reached 77.8° W.

For NH_3, whose continental sources included combustion and biological processes (from south of Atacama desert), we expect it was quantitatively sequestered on the acidic SO_4^{2-} aerosols as NH_4^+. Consequently, the fractional decrease of $[NH_4^+]$ across the longitude should be identical to that of $[SO_4^{2-}]$, which was found to be the case east of 71.5° W as these internally mixed aerosol components were diluted/removed together. If we consider the emissions impacting this eastern region were dominated by combustion sources and had little biological input, a minimum emission factor of $[NH_3]/[CO] \sim 0.02$ (ppb ppb^{-1}) is estimated because of removal that has already taken place. However, west of 71.5° W increased amount of NH_4^+ relative to SO_4^{2-} was observed peaking at ~ 73.7° W, suggesting additional sources in air masses from further to the south, either of oceanic or continental, or both. We suggest that an oceanic source is plausible based on composite vertical distributions (see below). This increased NH_4^+ over SO_4^{2-} (Fig. 19a) gave rise to an additional neutralization of the SO_4^{2-} aerosols between 72° W and 77° W (Fig. 10).

Org also showed a fractional decay rate nearly identical to that of SO_4^{2-} east of 72° W. However, unlike NH_4^+, [Org] is known to increase with photochemical age of emissions due to the formation of secondary organic aerosols (SOA). Based on CO emission factor, Kleinman et al. (2008) found a proportionality of ~ 60 $\mu g\,m^{-3}$ Org per ppm of CO in photochemically aged air applicable to urban emissions. The maximum estimated is $[Org]_{max} \sim 0.84\,\mu g\,m^{-3}$ corresponding to a $[CO]_{ex} \sim 14$ ppb. Since the observed [Org] ~ 0.25 $\mu g\,m^{-3}$ was only ~ 1/3 of the estimated maximum at the easternmost longitude, it appears that a large portion of the Org had already been removed from the aged air.

ACPD
13, 26043–26115, 2013

The fact that Org decreased at a fractional rate identical to that of SO_4^{2-} east of 72° W is consistent with the scenario that Org and SO_4^{2-} aerosols were internally mixed and formation was negligible because the air masses were well aged. (For the westermost point where $[CO]_{ex} \sim 6$ ppb, the expected [Org] $\sim 0.36\,\mu g\,m^{-3}$, but the observed was $\sim 0.09\,\mu g\,m^{-3}$, suggesting ~ 75 % of the maximum Org that could be formed had been lost assuming, a magnitude similar to that for SO_4^{2-}.)

Regarding NO_3^-, which is a stable product of oxides of nitrogen with a characteristic time against oxidizing by the OH radicals of ~ 1 day at $[OH] \sim 5 \times 10^{-7}\,cm^{-3}$, and is the predominant nitrogen species in aged air. At the easternmost longitude, we estimate a $[NO_y]$ of ~ 1.4 ppb for $[CO]_{ex} = 14$ ppb based on an urban emission ratio of $[CO]/[NO_y] \sim 10$ dominated by vehicles (Parrish, 2006), noting that this ratio can be higher for an older vehicle fleet. The observed median NO_3^- concentration found in SSA particles was only ~ 0.08 ppb, again indicating that nearly half of the nitrogen species had already been lost. It is reasonable to suggest from this observation that SO_4^{2-}, NH_4^+, and Org aerosols were internally mixed and therefore removed/diluted at the same rate. However, the fact that NO_3^- aerosol also showed the same decay rate as SO_4^{2-} indicates the SSA on which NO_3^- was absorbed were removed/diluted at the same rate as SO_4^{2-} aerosols for particles $D_p \leq 1.5\,\mu m$. The fractional decay rates of SO_4^{2-} and NO_3^- aerosols continue to track each other to ~ 78° W with SO_4^{2-} showing a slight elevation over NO_3^- between 72° W and 74° W indicating possible source variations in which SO_4^{2-} emission had increased over NO_3^-. CO also revealed a slight increase between 72° W and 74° W due possibly to variations in source attributes. We note that while SO_4^{2-} and NO_3^- continue to decrease at approximately the same rates west of ~ 72° W, decays of NH_4^+ and Org significantly slowed down, reflecting additional sources of these species relative to SO_4^{2-}. In contrast, the increase in OA started at ~ 72° W and remained unabated to ~ 78° W, where it provided more than twice as much Org than associated with SO_4^{2-} from combustion. This increase in Org is un-

ACPD
13, 26043–26115, 2013

likely to result from entrainment of FT air since the median Org concentrations in the FT and the MBL were comparable, and the MBL SO_4^{2-} to NO_3^- ratio in this region did not vary (noting that NO_3^- is all but absent in the FT air). Because the transects west of ~ 72° W received emissions from coastal regions south of 31° S (Allen et al., 2011) where biogenic emissions are expected, this increased OA (normalized to CO) over that observed on transect east of ~ 72° W can be reasonably attributed to these land sources. Although oceanic organic sources cannot be completely ruled out, we consider they play only a minor role at best unless a clear bifurcation in productivity, higher west of ~ 72° W, can be supported. In fact, the lower ocean surface temperatures associated high productivity upwelling zone were found near the coast (Rahn and Garreaud, 2010) is inconsistent with this possibility. Ratios of Org to $SO_4^{2-} \leq 0.08$ used to infer a marine origin by Shank et al. (2011) is shown in Fig. 19b as a function of longitude; the median $[Org]/[SO_4^{2-}] = 0.13$ at ~ 78° W corresponding to a median [CO] of 68 ppb, indicating significant land influence. For data points associated with [CO] < 62 ppb (in color, Fig. 19b) we note most of the Org/SO_4^{2-} ratios exceeded that suggested of clean marine atmosphere for the SEP region. We consider a continental source that had a minimal CO input, i.e., biogenic emissions from vegetation are plausible.

4.6 Composite vertical distributions of aerosol and gas constituents

The LOWESS fits of the vertical distributions of SO_4^{2-}, NH_4^+, and Org in Fig. 7, and Na^+ in Fig. 8 are normalized to their respective values at the lowest altitude, exhibiting apparent profiles (Fig. 20) that also reflect the G-1 sampling bias (e.g., greater near the shore at ~ 500 m than other altitudes). Even though these composite patterns do not represent vertical distributions like soundings, we nonetheless can gain insights into sources and tranport of the chemical constituents by comparing their relative trends. In Fig. 20, SO_4^{2-} and Org display very similar vertical patterns in the lower MBL, but diverged in the upper MBL with SO_4^{2-} decreasing faster with altitude than Org.

ACPD
13, 26043–26115, 2013

We attribute their similar trends in the lower MBL to similar source attributes in which SO_4^{2-} and Org aerosols/precursors were either co-emitted or co-located. The slower decrease of Org than SO_4^{2-} with altitude in the upper MBL (Fig. 20b) could in principle be due to mixing of FT air which was more enriched in Org than SO_4^{2-} (Fig. 7). However, the importance of this process can be ruled out based on the vertical distribution of SSA which showed minimal influence of the FT air. Two other possibilites include (1) in-cloud production (Blando and Turpin, 2000) that favored Org compared to SO_4^{2-}, especially if SO_2 had been depleted in the air that was sampled, and (2) a preferential removal of SO_4^{2-} over Org by precipitation if SO_4^{2-} and Org aerosols were externally mixed. Although organic and SO_4^{2-} aerosols from urban and industry are believed to be internally mixed, the extra OA from biogenic sources from coastal land south of 31° S has a potential to be externally mixed with anthropogenic SO_4^{2-} aerosols if primary OA, such as that from biomass burn, dominates. Consequently, both the two latter possibilites are conceivable and it is not possible to assess their relative importance. On the other hand, CO and O_3 were nearly uniformly distributed (Fig. 20b), consistent with their longer life times that allowed them to be well mixed in the MBL.

The vertical distribution of NH_4^+ showed an overall trend similar to SO_4^{2-} and Org, but with a steeper increase with altitude than that of SO_4^{2-} in the lower MBL. This observation can potentially result from either a source or a sink of NH_3 at the ocean surface. Since the SO_4^{2-} aerosols were strongly acidic, losing NH_3 from the acidic SO_4^{2-} aerosol to the mildly basic sea water can be ruled out, and this sharp gradient suggests an oceanic NH_3 source. Positive sea-to-air NH_3 flux has been observed for parts of the oceans (Johnson et al., 2008), especially in low latitude coastal regions with high productivity. We note that aerosol NH_4^+ showed a maximum at ~ 260 m, below that of SO_4^{2-}, reflecting an optimum rate of sequestering of NH_3 due to the maximum availability of both SO_4^{2-} aerosol and gaseous NH_3. Above ~ 260 m, NH_4^+ started to decrease as NH_3 became the limiting reagent despite the continous increase of SO_4^{2-} aerosol till ~ 500 m. The decrease in NH_4^+ with altitude in the upper MBL is more gradual than that

ACPD
13, 26043–26115, 2013

of SO_4^{2-}. This small increasing trend of $[NH_4^+]/[SO_4^{2-}]$ ratio indicates that in-cloud SO_4^{2-} production was not evident in the G-1 study region as NH_4^+ was conserved.

Distinct from SO_4^{2-} and Org, Na^+ (representing SSA with $D_p \leq 2\,\mu m$) showed a much more uniform vertical distribution with a small decreasing trend with altitude. Unlike continentally derived aerosols which displayed a strong land to sea gradient, SSA loading in the MBL remained relatively constant across the longitude and therefore exhibits a composite vertical distribution that is less prone to sampling biases. Since SSA particles with $D_p \leq 2\,\mu m$ are expected to be uniformly mixed vertically, this small gradient may in principle reflect dilution due to entrainment of FT air, loss due to precipitation removal, or the RH effect on SSA particle sizes discussed earlier. Since the observed difference of a factor of 2 between the top and the bottom of the MBL can be readily accounted for by the RH effect on SSA particle size, we rule out the importance of entrainment of FT air and precipitation scavenging. In view of this, one could consider using a sounding of MBL sub-micron SSA as a tracer under non-precipitating conditions to estimate the extent of entrainment mixing from the FT. Submicron SO_4^{2-} and Org aerosols are less suitable as tracers because of confounding factors such as possible in-cloud formation and input from FT air. Finally, we note that the Na^+ vertical profile exhibited a small minimum at ~ 260 m that corresponded to a small maximum in the profiles of both water mixing ratio and potential temperature, but not in that of SO_4^{2-} and Org. We believe this apparent "inversion" is an artifact due to the sampling pattern, and does not reflect a true physical layering.

4.7 Sources of organic aerosols

PMF analysis (Ulbrich et al., 2009) is performed on organic mass spectra obtained with the AMS to gain understanding of the sources of OA. We use the data of 28 October 2008 and 6 November 2008 as they covered the widest longitudinal range, maximizing the chance to reveal the contrast between polluted and cleaner MBL. By minimizing the scaled residual (Q/Q_{exp}) as a function of P (factor) and F_{peak} (matrix rotation), we

ACPD
13, 26043–26115, 2013

identified mass spectral profiles that are physically realistic, and time series that can be rationalized in terms of location and other concomitant observations. We first examine the results from a minimum number of factors. Data of 28 October 2008 with $P = 3$ and $F_{peak} = 0.2$ (Fig. 21) show factors 1 and 2 as oxygenated OA (OOA) and hydrocarbon-like OA (HOA), respectively. Factor 3 is due to contaminants from silicone conductive tubing (Schneider et al., 2006; Timko et al., 2009). The suggestion that these contaminant signals arise from deposition of dimethylsiloxane vapor onto soot particles (Schneider et al., 2006) cannot be tested here as the loadings of soot particles during VOCALS were too small to be quantified by a particle soot absorption photometer deployed on the G1 (LOD $\sim 1.5\,\mathrm{M\,m^{-1}}$).

To corroborate the HOA and OOA factors, we compare their time series to those for CO and SO_4^{2-} (Fig. 21a) whose concentrations are related to primary emissions and secondary products, respectively (Zhang et al., 2011). CO and HOA were well correlated during the inbound leg in the MBL (Fig. 21a), lending support to the HOA factor. This correlation was absent during in-cloud and AC segments in the out-bound leg: in the former aerosol-turned cloud droplets were not sampled, and in the latter FT air masses had different origins. In this connection, we note a significant gradient in FT CO, with high concentrations near the shore that decreased sharply with offshore distance. This suggests that close-by sources from the South America continent can be transported to higher altitudes near the shore. However, FT CO was much lower west of $\sim 74^{\circ}$ W on 28 October 2008, indicating cleaner air and a diminishing impact of closeby sources. OOA was correlated with SO_4^{2-} albeit at two different OOA/SO_4^{2-} ratios, lower near the shore (~ 0.09) and higher off shore (~ 0.2), reflecting possibly different source attributes. Being correlated with SO_4^{2-}, this OOA is thought to represent low volatility OA (e.g. Jimenez et al., 2009). The "extra" OOA based on a higher OOA/SO_4^{2-} ratio observed offshore suggests that the additional OA from the south was likely of biogenic origin without concomitant sulfur emissions. Since there was no indication of "extra" CO in the MBL based on the correlation between CO and the HOA, downward mixing of FT air as a source of OOA is unlikely. The PMF results of the 6 November 2008 data

ACPD
13, 26043–26115, 2013

with $P = 4$ and $F_{peak} = 0.6$ show factor 1, OOA, has a profile nearly identical to that of 28 October 2008, and the OOA/SO_4^{2-} ratio also increases with distance from the shore (Fig. 22a). Factor 2 however indicates an oxidized OA rather than the HOA found as factor 2 in 28 October 2008 data, with a mass spectrum resembling semi-volatile OOA typically found in urban areas (e.g., Zhang et al., 2005; Ng et al., 2010), which showed no correlation with CO (Fig. 22a). Factor 3 resembles fresh emissions encountered during take off and landing; factor 4 represents silicone tubing contaminants, but with additional mass fragments near m/z 280 of unknown origin (Fig. 22a).

The absence of HOA factor on 6 November 2008 is intriguing in view of the presence of a fairly substantial CO concentration of 70 ppb or greater, comparable to that of 28 October 2008. According to Allen et al. (2011, Fig. 4 therein), MBL air trajectories ending at 20 S parallel were remarkably consistent during VOCALS, the southerly to southeasterly winds bringing significant coastal emissions to the marine atmosphere up to 80° W. The lack of HOA on 6 November 2008 may therefore reflect an enhanced processing of the emissions due to either increased reaction rates or reaction time, or both, significantly reducing HOA. In this regard, Allen et al. (2011) suggested that variations in emissions may be responsible for the observed divergence in concentrations. Regarding reaction time, the wind speeds on 6 November 2008 (3–7 $m\,s^{-1}$) were slower than on 28 October 2008 (2–11 $m\,s^{-1}$), possibly leading to a longer processing time of the air masses sampled on 6 November 2008. We recognize the local wind data can only be used as inference for the recent past history. However, the fact that wind fields in SEP had been highly uniform during VOCALS (Rahn and Garreaud, 2010) may lend credence to this possibility. Regarding increased reaction rates, we recognize that cloud processing is a plausible contributing factor in SEP and may have played a more important role on the air mass observed on 6 November 2008 than that on 28 October 2008. Although the extent of cloud processing prior to sampling is difficult to assess, cloud processing is inferred from a bi-modal particle size distribution marked by a so-called Hoppel minimum (Hoppel et al., 1986). We discuss this possibility in a later section.

ACPD
13, 26043–26115, 2013

4.8 Identification of organosulfur compounds

The OOA mass spectra identified for both 28 October 2008 and 6 November 2008 flights, which resembles that for fulvic acid, also contain mass fragments m/z 79 ($CH_3SO_2^+$) and m/z 96 ($CH_3SO_3H^+$), indicative of MSA (Phinney et al., 2006; Zorn et al., 2008). Since MSA is a product of DMS which serves as the most important precursor of marine SO_4^{2-} aerosol, its characterization is crucial for understanding DMS's contribution to the marine environment. In terms of detection, we keep in mind that any MSA produced in the gas phase is expected to be squestered in SSA particles (e.g., Hopkins et al., 2008) as refractory sodium salt, exhibiting low CE. Attempting to isolate a MSA factor, we repeated the PMF analyses on 28 October 2008 and 6 November 2008 data using $P = 5$ (Fig. 23) and $P = 6$ (Fig. 24), respectively, that were found necessary to separate the MSA factor, although the highest factor in each analysis was of unknown chemical nature in minute amounts. Comparison of the MSA factor with a MSA mass spectrum obtained on an AMS (Phinney et al., 2006) showed a high degree of correspondence, recognizing that the m/z 48 and m/z 64 signals are missing because they have been removed by the AMS algorithm for SO_4^{2-} quantification. The m/z 81 (SO_3H^+) was the only major fragment missing from both MSA mass spectrum profiles, suggesting the absence of acidic MSA. The MSA mass spectrum factors obtained from the two different flights showed a strong correlation (Fig. 25), even though fragments m/z 12 and m/z 45 appeared only on 28 October 2008 but not on 6 November 2008 perhaps due to a lessed cloud processing of the former. Based on these considerations, we conclude that there is a strong likelyhood that the MSA factor represents the MSA species. However, while we are unsure of the CE of MSA which was presumably SSA particle bound, we assert that it was not derived from oceanic DMS. We note the longitudinal distributions of MSA (the time series profile) observed on both 28 October 2008 and 6 November 2008 were strongly correlated with SO_4^{2-} (Fig. 23 and Fig. 24) west of 73° W, suggesting co-emitted or co-located sources of these two species and/or their precursors. Although this correlation appeared to be missing east

ACPD
13, 26043–26115, 2013

of 73° W on both days, a similar trend in MSA and SO_4^{2-} could be discerned albeit with a gradually increasing MSA to SO_4^{2-} ratio with distance from the shore. Although MSA has been extensively investigated as a marine atmosperhic constituent from DMS oxidation, its presence in continental air has not been characterized in detail. Hueber et al. (1996) reported a higher level of MSA in polluted air advected from the continent than in air of marine origin, but did not examine continental sources as one of the possible explanations.

Another plausible organosulfur compound that could explain this MSA factor, is hydroxymethanesulfonic acid (HMSA). Produced in the liquid phase (e.g., in-cloud) from S(VI) and formaldehyde, HMSA is found near source regions in aerosol particles (Dixon and Aasen, 1999) as well as in cloud and fog waters (Munger et al., 1984; Rao and Collett Jr., 1995; Dall'Osto et al., 2009). HMSA is stable under acidic conditions and decomposes to HSO_3^- and H_2CO at a rate constant of 4.8 $(-7)\,s^{-1}$ and 3.5 $(-6)\,s^{-1}$ at pH = 4 and pH = 5, respectively (Kok et al., 1986), corresponding to a characteristic time of ~ 80 h at pH = 5, and longer at lower pH. Although HMSA seems not consistent with the m/z 15 methyl fragment found in the MSA mass spectrum, we cannot completely rule out this candidate until its mass spectrum is firmly established on the AMS. We note that Hawkins et al. (2010) have identified organosulfates during VOCALS that were correlated with acidic aerosol sulfate originating from the continent. Since organosulfate formation involves acid catalysis (Surratt et al., 2008), we expect this product to be present in the non-refractroy acidic sulfate particles and therefore detected by the AMS. The identification of organosulfate is based on C-O-S stretching at 876 cm^{-1} representing esters of either sulfate or sulfite (Maria et al., 2003). The MSA factor mass spectrum may be explained by a methyl ester of sulfonic acid as an organosulfate, whose mass spectrum on the AMS should aid the interpretation of the data observed here.

The mass spectrum of factor 1 resembles fulvic acid, oxalic acid (Alfarra, 2004), aerosols from smoldering fir and beech fires (Weimer et al., 2008), as well as that of a factor identified as continental in origin, all being extensively oxidized (Chang et.,

ACPD
13, 26043–26115, 2013

2011). We note that this factor was responsible for the increased OOA/SO_4^{2-} ratio with distance from the shore, reflecting the increased OA contribution relative to SO_4^{2-} in air masses from coastal regions further to the south. This extra OOA over that of urban and industry sources may be attributed to either a direct input from biomass burning (Chand et al., 2010) or to secondary production from biogenic VOC emissions (Tsapakis et al., 2002). However, it is interesting to point out that while the MSA factor was detected exclusively in the MBL, the fulvic acid factor was also found in FT on 28 October 2008 (Fig. 23b). The presence of aged OOA in FT is consistent with long range transport of biomass burn plumes to the VOCALS domain described by Allen et al. (2011).

4.9 Cloud processing

In this section we examine possible evidence for more extensive cloud processing on 8 November 2008 compared to that on 28 October 2008 to help explain the absence of HOA in the former. We compare the particle size distributions measured by the DMA during the return legs in the MBL on these two flights as a function of longitude with data binned into 1-degree intervals (Fig. 26). The data from both flights exhibited the bi-modal distribution expected of cloud processing consistent with the composite distribution of the entire G-1 mission (Kleinman et al., 2012), with the exception of those sampled closest to the shore on both flights. We consider the size distribution observed between 71° W and 72° W to be representative of the emissions impacting the MBL observed on this flight westward of this longitude based on the similarity in mode sizes and concentration levels. The much higher Aitken mode particle concentrations compared to the droplet mode reflects the emission characteristics as well as the limited cloud processing due to both a shorter processing time and a lack of clouds in the mid-afternoon near the shore when they were sampled. The particle size distributions from east to west on 28 October 2008 were highly uniform evidenced by a near constant droplet mode size at 0.18 µm and a progressively smaller Aitken mode size from ~ 0.06 to ~ 0.04 µm, reflecting emissions similar in characteristics that were more ex-

ACPD
13, 26043–26115, 2013

tensive processed and diluted going west along the ~ 19° S parallel. The spectrum for the westernmost section, 77° W–77.3° W, showed some cloud contamination reflected in the increased small size particles from shattering, which however did not affect the mode sizes. In comparison, the data of 6 November 2008 showed still less processed emissions between 71° W and 72° W indicated by the much higher Aitkin mode particle concentrations compared to that of the droplet mode with only a slight hint of the Hoppel minimum. The Aitkin mode size decreased progressively from ~ 0.07 µm to ~ 0.04 µm from east to west similar to that observed on 28 October 2008. Regarding droplet mode particle size distributions, we note the concentrations decreased rapidly and steadily from east to west on 28 October 2008, but this decrease was much less pronounced on 6 November 2008 (Fig. 26). We surmise this rather steady droplet mode particle concentrations observed on 6 November 2008 across a wide longitude range was due to a more extensive cloud processing, growing more particles into the larger particle size range. The lower WS on 6 November 2008 compared to that of 28 October 2008 could allow a more extensive cloud processing because of an increased transport and reaction time. Finally, the droplet mode particle size is seen to decrease with distance from the shore on 6 November 2008, noting that while the left edges of the peaks were tightly clustered together, the right edges steadily retracted. In contrast, the droplet mode particle size observed on 28 October 2008 remained roughly constant as the number concentrations steadily decreased from east to west. We attribute this size shift observed on 6 November 2008 to the loss of larger sized particles to precipitation which may also be consistent with a more extensive cloud processing.

5 Conclusions

Chemical composition of accumulation mode particles in coastal marine atmospheres off northern Chile was determined on board the DOE G-1 using an AMS and the PILS-IC during 2008 VOCALS-REx. Strongly acidic sulfate aerosols, which were on average only 25 % neutralized by NH_3, dominated all other aerosol constituents, accounting for

ACPD
13, 26043–26115, 2013

≥ 50 % of the total aerosol mass concentration; total organic aerosol (Org) and NH_4^+ each contribued only < 15 %. Aerosol NO_3^- was found to reside on SSA particles, externally mixed with SO_4^{2-} particles, resulting from uptake of gaseous HNO_3 by SSA giving rise to a portion of the observed chloride deficit. Concentrations of MBL aerosol SO_4^{2-}, NH_4^+, Org, and NO_3^- all exhibited a strong longitudinal gradient decreasing with distance from the shore, consistent with their continental origins. In contrast, SSA loading represented by Na^+ was fairly uniform in the MBL with a slight increase off shore where wind speeds were higher. The observed SSA mass loading agreed with the cannonical wind speed dependence reported in the literature; the coastal surf zone SSA production was found to contribute to SSA loading at distances as far as to ∼ 400 km offshore. Number concentration of SSA was much smaller than that for SO_4^{2-} aerosols even at ∼ 78° W, ∼ 800 km from the shore. Accumulation mode SSA loading showed a uniform vertical distribution and can in principle be used as a tracer to assess the extent of dilution of MBL due to entrainment of FT air. MSA, an oxidation product of DMS, was all but absent, indicating a minimal role played by DMS from the ocean in sulfur chemistry within the G-1 study domain. Relative changes in distribution patterns in simultaneously measured aerosol species suggest that sources beyond those from urban and industrial regions exist for NH_3, likely of oceanic origin, and for OA, likely from continental biogenic sources south of Acatama desert. In contrast, concentrations of MBL aerosol NO_3^- and SO_4^{2-} tracked each other and appeared to be entirely attributable to continental anthropogenic emissions that were co-emitted or co-located. PMF analysis of OA mass spectra obtained using the AMS showed an HOA on 28 October 2008 that was well correlated with CO, which was however absent on 6 November 2008. We attributed this contrast to a greater extent of cloud processing of the air masses observed on 6 November 2008. A highly oxidized OOA factor correlated with SO_4^{2-} was indentified for both flights. The ratio of OOA to SO_4^{2-} was lower near the coast and higher away from the shore because of an increased OOA derived from coatal biogenic emissions south of 31° S. Another OOA factor identified as an organosulfur, possibly

ACPD
13, 26043–26115, 2013

MSA, was also strongly correlated with SO_4^{2-} therefore believed to be of anthopogenic origin. Identity of this MSA factor, possibly including hydroxymethanesulfonic acid and methyl sulfonate, need to be investigated to better understand the transport of S(IV)-aldehydes adducts as sources for remote regions and the formation of organosulfur compounds as SOA.

Acknowledgements. The Atmospheric Sciences Program within the DOE Office of Biological and Environmental Research, which has since been merged into the Atmospheric System Research Program, supported this research. The authors gratefully acknowledge the DOE G-1 flight crew led by Chief Pilot Bob Hannigan for their dedication and professionalism that ensured a safe and productive scientific mission.

References

Allen, G., Coe, H., Clarke, A., Bretherton, C., Wood, R., Abel, S. J., Barrett, P., Brown, P., George, R., Freitag, S., McNaughton, C., Howell, S., Shank, L., Kapustin, V., Brekhovskikh, V., Kleinman, L., Lee, Y.-N., Springston, S., Toniazzo, T., Krejci, R., Fochesatto, J., Shaw, G., Krecl, P., Brooks, B., McMeeking, G., Bower, K. N., Williams, P. I., Crosier, J., Crawford, I., Connolly, P., Allan, J. D., Covert, D., Bandy, A. R., Russell, L. M., Trembath, J., Bart, M., McQuaid, J. B., Wang, J., and Chand, D.: South East Pacific atmospheric composition and variability sampled along 20° S during VOCALS-REx, Atmos. Chem. Phys., 11, 5237–5262, doi:10.5194/acp-11-5237-2011, 2011.

Alfarra, R.: Insights into Atmospheric Organic Aerosols Using an Aerosol Mass Spectrometer, Ph.D. Thesis, University of Manchester, 2004.

Benedict, K. B., Lee, T., and Collett Jr., J. L.: Cloud water composition over the Southeastern Pacific Ocean during the VOCALS Regional Experiment, Atmos. Environ., 46, 104–114, 2012.

Blando, J. D. and Turpin, B. J.: Secondary organic aerosol formation in cloud and fog droplets: a literature evaluation of plausibility, Atmos. Environ., 34, 1623–1632, 2000.

Brechtel, F.: Description and Assessment of a New Aerosol Inlet System for the DOE G-1 Research Aircraft, Technical Report, Brechtel Manufacturing, Inc., 2002.

Bretherton, C. S., Wood, R., George, R. C., Leon, D., Allen, G., and Zheng, X.: Southeast Pacific stratocumulus clouds, precipitation and boundary layer structure sampled along 20° S during VOCALS-REx, Atmos. Chem. Phys., 10, 10639–10654, doi:10.5194/acp-10-10639-2010, 2010.

Canagaratna, M. R., Jayne, J. T., Jimenez, J. L., Allan, J. D., Alfarra, R., Zhang, Q., Onasch, T. B., Drewnick, F., Coe, H., Middlebrook, A., Delia, A., Williams, L. R., Trimborn, A. A., Northway, M. J., DeCarlo, P. F., Kolb, C. E., Davidovits, P., and Worsnop, D. R.: Chemical and microphysical characterization of ambient aerosols with the aerodyne aerosol mass spectrometer, Mass Spectrom. Rev., 26, 185–222, doi:10.1002/mas.20115, 2007.

Chand, D., Hegg, D. A., Wood, R., Shaw, G. E., Wallace, D., and Covert, D. S.: Source attribution of climatically important aerosol properties measured at Paposo (Chile) during VOCALS, Atmos. Chem. Phys., 10, 10789–10801, doi:10.5194/acp-10-10789-2010, 2010.

Chang, R. Y.-W., Leck, C., Graus, M., Müller, M., Paatero, J., Burkhart, J. F., Stohl, A., Orr, L. H., Hayden, K., Li, S.-M., Hansel, A., Tjernström, M., Leaitch, W. R., and Abbatt, J. P. D.: Aerosol composition and sources in the central Arctic Ocean during ASCOS, Atmos. Chem. Phys., 11, 10619–10636, doi:10.5194/acp-11-10619-2011, 2011.

Cleveland, W. S.: Robust locally weighted regression and smoothing scatterplots, J. Am. Stat. Assoc., 74, 829–836, 1979.

Dall'Osto, M., Harrison, R. M., Coe, H., and Williams, P.: Real-time secondary aerosol formation during a fog event in London, Atmos. Chem. Phys., 9, 2459–2469, doi:10.5194/acp-9-2459-2009, 2009.

Dixon, R. W. and Aasen, H.: Measurement of hydroxymethanesulfonate in atmospheric aerosols, Atmos. Environ., 33, 2023–2029, 1999.

Drewnick, F., Hings, S. S., DeCarlo, P., Jayne, J. T., Gonin, M., Fuhrer, K., Weimer, S., Jimenez, J. L., Demerjian, K. L., Borrmann, S., and Worsnop, D. R.: A new Time-of-Flight Aerosol Mass Spectrometer (TOF-AMS) – instrument description and first field deployment, Aerosol Sci. Tech., 39, 637–658, doi:10.1080/02786820500182040, 2005.

Haller, A. G., Strawa, A. W., Schmid, B., Andrews, E., Ogren, J., Sheridan, P., Ferrare, R., Covert, D., Elleman, R., Jonsson, H., Bokarius, K., and Luu, A.: Atmospheric radiation measurements aerosol intensive operating period: comparison of aerosol scattering during coordinated flights, J. Geophys. Res., 111, D05S09, doi:10.1029/2005JD006250, 2006.

Hawkins, L. N., Russell, L. M., Covert, D. S., Quinn, P. K., and Bates, T. S.: Carboxylic acids, sulfates, and organosulfates in processed continental organic aerosol over the

ACPD
13, 26043–26115, 2013

Southeast Pacific Ocean during VOCALS-Rex 2008, J. Geophys. Res., 115, D13201, doi:10.1029/2009JD013276, 2010.

Hopkins, R. J., Desyaterik, Y., Tivanski, A. V., Zaveri, R. A., Berkowitz, C. M., Tyliszczak, T., Gilles, M. K., and Laskin, A.: Chemical speciation of sulfur in marine cloud droplets and particles: analysis of individual particles from the marine boundary layer over the California current, J. Geophys. Res., 113, D04209, doi:10.1029/2007JD008954, 2008.

Hoppel, W. A., Frick, G. M., and Larson, R. E.: Effect of nonprecipitating clouds on the aerosol size distribution in the marine boundary layer, Geophys. Res. Lett., 13, 125–128, doi:10.1029/GL013i002p00125, 1986.

Huebert, B. J., Zhuang, L., Howell, S., Noone, K., and Noone, B.: Sulfate, nitrate, methanesulfonate, chloride, ammonium, and sodium measurements from ship, island, and aircraft during the Atlantic Stratocumulus Transition Experiment/Marine Aerosol Gas Exchange, J. Geophys. Res. Atmos., 101, 4413–4423, doi:10.1029/95JD02044, 1996.

Jayne, J. T., Leard, D. C., Zhang, X., Davidovits, P., Smith, K. A., Kolb, C. E., and Worsnop, D. R.: Development of an aerosol mass spectrometer for size and composition analysis of submicron particles, Aerosol Sci. Tech., 33, 49–70, doi:10.1080/027868200410840, 2000.

Jiminez, J. L., Canagaratna, M. R., Donahue, N. M., Prevot, A. S. H., Zhang, Q, Kroll, J. H., DeCarlo, P. F., Allan, A. C., Coe, H., Ng, N. L., Aiken, A. C., Docherty, K. S., Ulrich, I. M., Grieshop, A. P., Robinson, A. L., Duplissy, J., Smith, J. D., Wilson, K. R., Lanz, V. A., Hueglin, C., Sun, Y. L., Tian, J., Laaksonen, A., Raatikainen, T., Vaattovaara, P., Ehan, M., Kulmula, M., Tomlinson, J. M., Collins, D. R., Cubison, M. J., Dunlea, E. J., Huffman, J. A., Onasch, T. B., Alfarra, M. R., Williams, P. I., Bower, K., Kondo, Y., Schneider, J., Drenwick, F., Borrman, S., Weimer, S., Demerjian, K., Salcedo, D., Cottrell, L., Griffin, R., Takami, A., Miyoshi, T., Hatakeyama, S., Shimono, A., Sun, J. Y., Zhang, Y. M., Dzepina, K., Kimmel, J. R., Sueper, D., Jayne, J. T., Herndon, S. C., Trimborn, A. M., Williams, L. R., Wood, E. C., Middlebrook, A. M., Kolb, C. E., Baltensperger, U., and Worsnop, D. R.: Evolution of organic aerosols in the atmosphere, Science, 326, 1525–1529, doi:10.1126/science.1180353, 2009.

Johnson, M. T., Liss, P. S., Bell, T. G., Lesworth, T. J., Baker, A. R., Hind, A. J., Jickells, T. D., Biswas, K. F., Malcolm, E., Woodward, S., and Gibb, S. W.: Field observations of the ocean-atmosphere exchange of ammonia: fundamental importance of temperature as revealed by a comparison of high and low altitudes, Global Geochem. Cycles, 22, GB1019, doi:10.1029/2007GB003039, 2008.

ACPD
13, 26043–26115, 2013

Kawakami, N., Osada, K., Nishita, C., Yabuki, M., Kobayashi, H., Hara, K., and Shiobara, M.: Factors controlling sea salt modification and dry deposition of nonsea-salt components to the ocean, J. Geophys. Res., 113, D14216, doi:10.1029/2007JD009410, 2008.

Kleinman, L. I., Daum, P. H., Lee, Y.-N., Senum, G. I., Springston, S. R., Wang, J., Berkowitz, C., Hubbe, J., Zaveri, R. A., Brechtel, F. J., Jayne, J., Onasch, T. B., and Worsnop, D.: Aircraft observations of aerosol composition and ageing in New England and Mid-Atlantic states during the summer 2002 NEAQS Field Campaign, J. Geophys. Res., 112, D09310, doi:10.1029/2006JD007786, 2007.

Kleinman, L. I., Springston, S. R., Daum, P. H., Lee, Y.-N., Nunnermacker, L. J., Senum, G. I., Wang, J., Weinstein-Lloyd, J., Alexander, M. L., Hubbe, J., Ortega, J., Canagaratna, M. R., and Jayne, J.: The time evolution of aerosol composition over the Mexico City plateau, Atmos. Chem. Phys., 8, 1559–1575, doi:10.5194/acp-8-1559-2008, 2008.

Kleinman, L. I., Daum, P. H., Lee, Y.-N., Lewis, E. R., Sedlacek III, A. J., Senum, G. I., Springston, S. R., Wang, J., Hubbe, J., Jayne, J., Min, Q., Yum, S. S., and Allen, G.: Aerosol concentration and size distribution measured below, in, and above cloud from the DOE G-1 during VOCALS-REx, Atmos. Chem. Phys., 12, 207–223, doi:10.5194/acp-12-207-2012, 2012.

Kok, G., Gitlin, S. N., and Lazrus, A. L.: Kinetics of the formation and decomposition of hydroxymethanesulfonate, J. Geophys. Res., 91, 2801–2804, 1986.

Kroll, J. H. and Seinfeld, J. H.: Chemistry of secondary organic aerosol: formation and evolution of low-volatility organics in the atmosphere, Atmos. Environ., 42, 3593–3624, 2008.

Lewis, E. R. and Schwartz, S. E.: Sea Salt Aerosol Production: Mechanisms, Methods, Measurements and Models, Geophysical Monograph Series, vol. 152, American Geophysical Union, Washington, DC, 413 pp., 2004.

Lin, P., Yu, J. Z., Engling, G., and Kalberer, M.: Organosulfates in humic-like substance fraction isolated from aerosols at seven locations in East Asia: a study by ultra-high-resolution mass spectrometry, Environ. Sci. Technol., 46, 13118–13127, 2012.

Maria, S. F., Russell, L. M., Turpin, B. J., Porcja, R. J., Campos, T. L., Weber, R. J., and Huebert, B. J.: Source signatures of carbon monoxide and organic functional groups in Asian Pacific Regional Aerosol Characterization Experiment (ACE-Asia) submicron aerosol types, J. Geophys. Res. Atmos., 108, 8637, doi:10.1029/2003JD003703, 2003.

ACPD
13, 26043–26115, 2013

Mathew, B. M., Middlebrook, A. M., and Onasch, T. B.: Collection efficiencies in an Aerodyne aerosol mass spectrometer as a function of particle phase for laboratory generated aerosols, Aerosol Sci. Tech., 42, 884–898, 2008.
Munger, J. W., Jacob, D. J., and Hoffmann, M. R.: The occurrence of bisulfite-aldehyde addition products in fog-and cloudwater, J. Atmos. Chem., 1, 335–350, 1984.
Ng, N. L., Canagaratna, M. R., Zhang, Q., Jimenez, J. L., Tian, J., Ulbrich, I. M., Kroll, J. H., Docherty, K. S., Chhabra, P. S., Bahreini, R., Murphy, S. M., Seinfeld, J. H., Hildebrandt, L., Donahue, N. M., DeCarlo, P. F., Lanz, V. A., Prévôt, A. S. H., Dinar, E., Rudich, Y., and Worsnop, D. R.: Organic aerosol components observed in Northern Hemispheric datasets from Aerosol Mass Spectrometry, Atmos. Chem. Phys., 10, 4625–4641, doi:10.5194/acp-10-4625-2010, 2010.
O'Dowd, C. D., Facchini, M. C., Cavalli, F., Ceburnis, D., Mircea, M., Decesari, S., Fuzzi, S., Yoon, Y. J., and Putaud, J.-P.: Biogenically driven organic contribution to marine aerosol, Nature, 431, 676–680, 2004.
Olsen, T. M. and Hoffmann, M. R.: Hydroxyalkylsulfonate formation: its role as a S(IV) reservoir in atmospheric water droplets, Atmos. Environ., 23, 985–997, 1989.
Orsini, D. A., Ma, Y., Sullivan, A., Sierau, B., Baumann, K., and Weber, R. J.: Refinements to the particle-into-liquid sampler (PILS) for ground and airborne measurements of water soluble aerosol composition, Atmos. Environ., 37, 1243–1259, 2003.
Parrish, D. D.: Critical evaluation of US on-road vehicle emission inventories, Atmos. Environ., 40, 2288–2300, 2006.
Phinney, L., Richard Leaitch, W., Lohmann, U., Boudries, H., Worsnop, D. R., Jayne, J. T., Toom-Sauntry, D., Wadleigh, M., Sharma, S., and Shantz, N.: Characterization of the aerosol over the sub-arctic North East Pacific Ocean, Deep-Sea Res. Pt. II, 53, 2410–2433, doi:10.1016/j.dsr2.2006.05.044, 2006.
Rahn, D. A. and Garreaud, R.: Marine boundary layer over the subtropical southeast Pacific during VOCALS-REx – Part 1: Mean structure and diurnal cycle, Atmos. Chem. Phys., 10, 4491–4506, doi:10.5194/acp-10-4491-2010, 2010.
Rao, X. and Collett Jr., J.: Behavior of S(IV) and formaldehyde in a chemically heterogeneous cloud, Environ. Sci. Technol., 29, 1023–1031, 1995.
Schneider, J., Weimer, S., Drewnick, F., Borrmann, S., Helas, G., Gwaze, P., Schmid, O., Andreae, M. O., and Kirchner, U.: Mass spectrometric analysis and aerodynamic properties of

ACPD
13, 26043–26115, 2013

various types of combustion-related aerosol particles, Int. J. Mass Spectrom., 258, 37–49, 2006.
Saide, P. E., Spak, S. N., Carmichael, G. R., Mena-Carrasco, M. A., Yang, Q., Howell, S., Leon, D. C., Snider, J. R., Bandy, A. R., Collett, J. L., Benedict, K. B., de Szoeke, S. P., Hawkins, L. N., Allen, G., Crawford, I., Crosier, J., and Springston, S. R.: Evaluating WRF-Chem aerosol indirect effects in Southeast Pacific marine stratocumulus during VOCALS-REx, Atmos. Chem. Phys., 12, 3045–3064, doi:10.5194/acp-12-3045-2012, 2012.
Schwartz, S. E.: Gas-aqueous reactions of sulfur and nitrogen oxides in liquid-water clouds, in: SO_2, NO and NO_2 Oxidation Mechanisms: Atmospheric Considerations, edited by: Calvert, J. G., Acid Precipitation Series, vol. 3, Butterworth, Boston, 173–208, 1984.
Shank, L. M., Howell, S., Clarke, A. D., Freitag, S., Brekhovskikh, V., Kapustin, V., McNaughton, C., Campos, T., and Wood, R.: Organic matter and non-refractory aerosol over the remote Southeast Pacific: oceanic and combustion sources, Atmos. Chem. Phys., 12, 557–576, doi:10.5194/acp-12-557-2012, 2012.
Slinn, W. G. N.: Air to sea transfer of particles, in: Air–Sea Exchange of Gases and Particles, edited by: Liss, P. S. and Slinn, W. G. N., D. Reidel Publishing Co., Dordrecht, Holland, 1983.
Springston, S. R., Kleinman, L. I., Nunnermacker, L. J., Brechtel, F., Lee, Y.-N., and Wang, J.: Chemical evolution of an isolated power plant plume during the TexAQs 2000 study, Atmos. Environ., 39, 3431–3443, 2005.
Surratt, J. D., Gómez-González, Y., Chan, A. W. H., Vermeylen, R., Shahgholi, M., Kleindienst, T. E., Edney, E. O., Offenberg, J. H., Lewandowski, M., Jaoui, M., Maenhaut, W., Claeys, M., Flagan, R. C., and Seinfeld, J. H.: Organosulfate formation in biogenic secondary organic aerosol, J. Phys. Chem. A, 112, 8345–8378, doi:10.1021/jp802310p, 2008.
Tang, I. N., Munkelwitz, H. R., and Davis, J. G.: Aerosol growth studies – II. Preparation and growth measurements of monodisperse salt aerosols, J. Aerosol Sci., 8, 149–159, 1977.
Timko, M. T., Yu, Z., Kroll, J., Jayne, J. T., Worsnop, D. R., Miake-Lye, R. C., Onasch, T. B., Liscinsky, D., Kirchstetter, T. W., Destaillats, H., Holder, A. L., Smith, J. D., and Wilson, K. R.: Sampling artifacts from conductive silicone tubing, Aerosol Sci. Tech., 43, 855–865, doi:10.1080/02786820902984811, 2009.
Tomlinson, J. M., Li, R., and Collins, D. R.: Physical and chemical properties of the aerosol within the southeastern Pacific marine boundary layer, J. Geophys. Res., 112, D12211, doi:10.1029/2006JD007771, 2007.

ACPD
13, 26043–26115, 2013

Tsapakis, M., Lagoudaki, E., Stephanou, E. G., Kavouras, I. G., Koutrakis, P., Oyola, P., and von Baer, D.: The composition and sources of $PM_{2.5}$ organic aerosol in two urban areas of Chile, Atmos. Environ., 36, 3851–3863, doi:10.1016/S1352-2310(02)00269-8, 2002.

Twohy, C. H., Anderson, J. R., Toohey, D. W., Andrejczuk, M., Adams, A., Lytle, M., George, R. C., Wood, R., Saide, P., Spak, S., Zuidema, P., and Leon, D.: Impacts of aerosol particles on the microphysical and radiative properties of stratocumulus clouds over the southeast Pacific Ocean, Atmos. Chem. Phys., 13, 2541–2562, doi:10.5194/acp-13-2541-2013, 2013.

Ulbrich, I. M., Canagaratna, M. R., Zhang, Q., Worsnop, D. R., and Jimenez, J. L.: Interpretation of organic components from Positive Matrix Factorization of aerosol mass spectrometric data, Atmos. Chem. Phys., 9, 2891–2918, doi:10.5194/acp-9-2891-2009, 2009.

Wang, J., Flagan, R. C., and Seinfeld, J. H.: A Differential Mobility Analyzer (DMA) system for submicron aerosol measurements at ambient relative humidity, Aerosol Sci. Tech., 37, 46–52, doi:10.1080/02786820300891, 2003.

Weimer, S., Alfarra, M. R., Schreiber, D., Mohr, M., Prévôt, A. S. H., and Baltensperger, U.: Organic aerosol mass spectral signatures from wood-burning emissions: influence of burning conditions and wood type, J. Geophys. Res. Atmos., 113, D10304, doi:10.1029/2007JD009309, 2008.

Wood, R., Mechoso, C. R., Bretherton, C. S., Weller, R. A., Huebert, B., Straneo, F., Albrecht, B. A., Coe, H., Allen, G., Vaughan, G., Daum, P., Fairall, C., Chand, D., Gallardo Klenner, L., Garreaud, R., Grados, C., Covert, D. S., Bates, T. S., Krejci, R., Russell, L. M., de Szoeke, S., Brewer, A., Yuter, S. E., Springston, S. R., Chaigneau, A., Toniazzo, T., Minnis, P., Palikonda, R., Abel, S. J., Brown, W. O. J., Williams, S., Fochesatto, J., Brioude, J., and Bower, K. N.: The VAMOS Ocean-Cloud-Atmosphere-Land Study Regional Experiment (VOCALS-REx): goals, platforms, and field operations, Atmos. Chem. Phys., 11, 627–654, doi:10.5194/acp-11-627-2011, 2011.

Yang, M., Huebert, B. J., Blomquist, B. W., Howell, S. G., Shank, L. M., McNaughton, C. S., Clarke, A. D., Hawkins, L. N., Russell, L. M., Covert, D. S., Coffman, D. J., Bates, T. S., Quinn, P. K., Zagorac, N., Bandy, A. R., de Szoeke, S. P., Zuidema, P. D., Tucker, S. C., Brewer, W. A., Benedict, K. B., and Collett, J. L.: Atmospheric sulfur cycling in the southeastern Pacific – longitudinal distribution, vertical profile, and diel variability observed during VOCALS-REx, Atmos. Chem. Phys., 11, 5079–5097, doi:10.5194/acp-11-5079-2011, 2011.

ACPD
13, 26043–26115, 2013

Yin, F., Grosjean, D., and Seinfeld, J. H.: Photooxidation of dimethyl sulfide and dimethyl disulfide. I: Mechanism development, J. Atmos. Chem., 11, 309–364, 1990.
Zhang, Q., Jimenez, J. L., Canagaratna, M. R., Ulbrich, I. M., Ng, N. L., Worsnop, D. R., and Sun, Y.: Understanding atmospheric organic aerosols via factor analysis of aerosol mass spectrometry: a review, Anal. Bioanal. Chem., 401, 3045–3067, doi:10.1007/s00216-011-5355-y, 2011.
Zorn, S. R., Drewnick, F., Schott, M., Hoffmann, T., and Borrmann, S.: Characterization of the South Atlantic marine boundary layer aerosol using an aerodyne aerosol mass spectrometer, Atmos. Chem. Phys., 8, 4711–4728, doi:10.5194/acp-8-4711-2008, 2008.

ACPD
13, 26043–26115, 2013

Table 1. Date and time of DOE G-1 research flights during VOCALS-REx[a].

Flight number	Date	Take-off	Land	Westernmost Point (Lon W)	Flight Duration
1	14 Oct 2008	15:52	18:53	72.4	3:01
2	17 Oct 2008	13:00	16:50	74.1	3:50
3	18 Oct 2008	13:07	15:16	72.6	2:09
4	22 Oct 2008	16:32	19:57	76.1	3:25
5	23 Oct 2008	12:49	16:35	73.1	3:45
6	25 Oct 2008	13:03	17:07	76.1	4:04
7	26 Oct 2008	13:01	16:36	75.1	3:35
8	28 Oct 2008	12:58	17:16	77.8	4:17
9	29 Oct 2008	15:58	19:33	72.0	3:35
10	01 Nov 2008	12:57	16:57	77.2	4:00
11	03 Nov 2008	12:58	16:51	74.1	3:53
12	04 Nov 2008	11:57	16:02	72.1	4:05
13	06 Nov 2008	11:57	16:21	77.9	4:23
14	08 Nov 2008	12:55	16:31	74.1	3:36
15	10 Nov 2008	13:02	16:50	75.2	3:47
16	12 Nov 2008	13:20	16:55	75.3	3:34
17	13 Nov 2008	12:54	16:42	76.8	3:47

[a] 18 October 2008 flight was aborted due to research power failure, missing most aerosol data.

ACPD
13, 26043–26115, 2013

Table 2. AMS Ionization Efficiency, normalization factor, and ratio of total mass to DMA volume.

Date	Ionization Efficiency ($\times 10^{-7}$)	Normalization Factor	Nss_tot/V_{DMA}
14 October			
17 October	2.9	1.70	1.94
18 October	1.9		
22 October	3.6	1.45	1.1
23 October	3.4	0.97	1.17
25 October	2.8	1.41	1.32
26 October	1.9	1.28	1.29
28 October	2.1	1.54	0.96
29 October		1.92	1.06
1 November	1.6	0.87	0.93
3 November		1.20	1.54
4 November	2.8	1.68	1.08
6 November		2.21	0.98
8 November		1.23	0.89
9 November[a]	3.82		
10 November		1.14	0.87
12 November	3.85	1.16	1.2
13 November		1.40	

[a] Ground study.

ACPD
13, 26043–26115, 2013

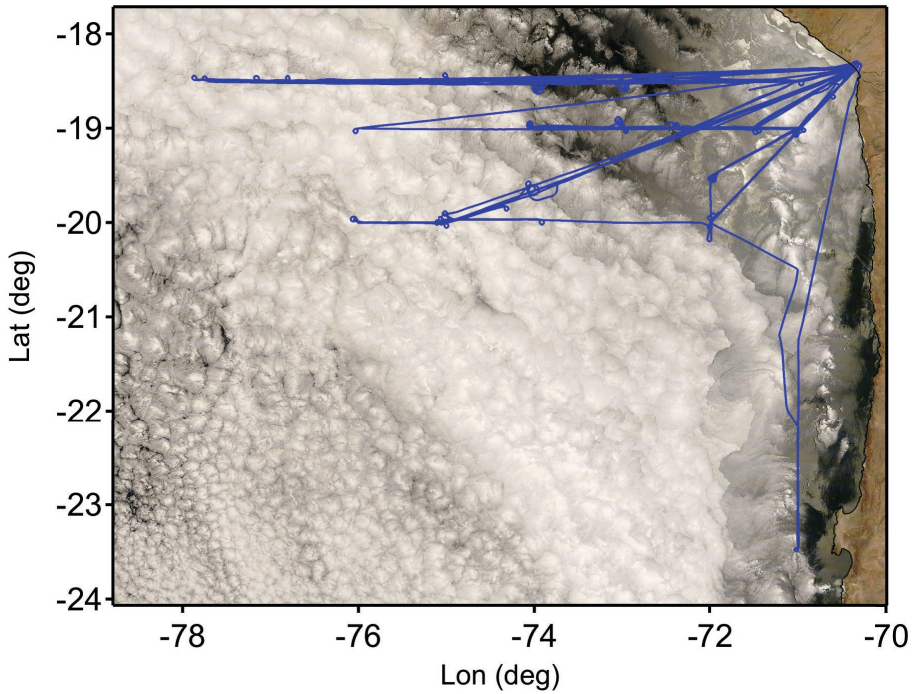

Fig. 1. Composite flight tracks of the DOE G-1 during 2008 VOCALS-REx overlaid on a Terra image taken at 16:50 UT 12 November 2008.

ACPD
13, 26043–26115, 2013

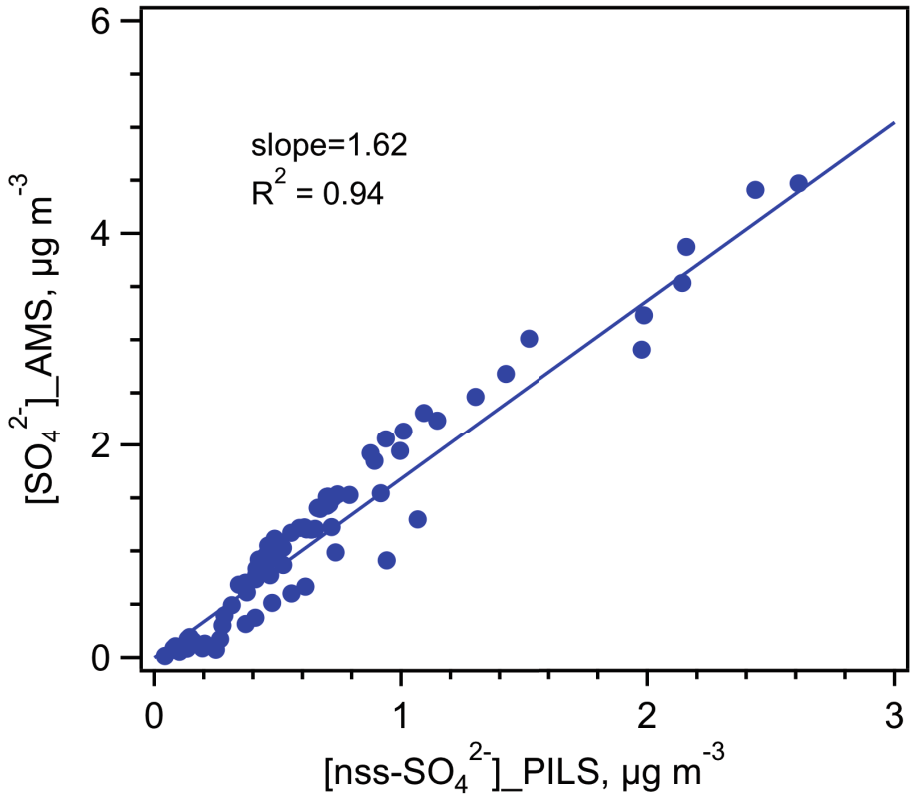

Fig. 2. Correlation of nss-SO_4^{2-} concentrations determined by the AMS and the PILS on 28 October 2008.

ACPD
13, 26043–26115, 2013

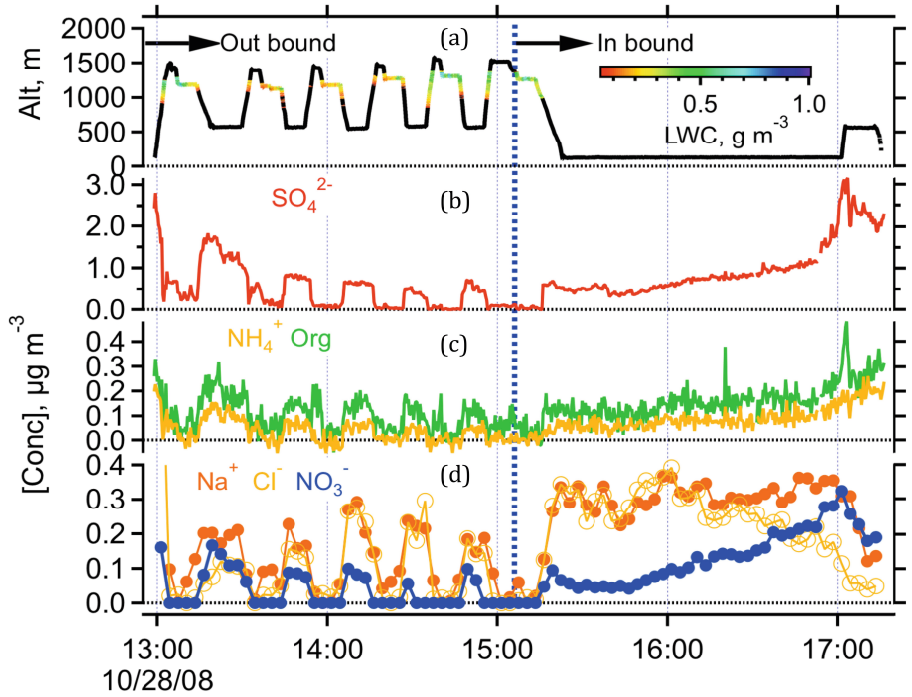

Fig. 3. Time plots of altitude and aerosol chemical concentrations measured on the 28 October 2008 flight. The aircraft altitude plot is color-coded to the liquid water content of clouds encountered during the out-bound leg (panel **a**); the blue dotted vertical line marks the time when the G-1 turned around and headed back to Arica.

ACPD
13, 26043–26115, 2013

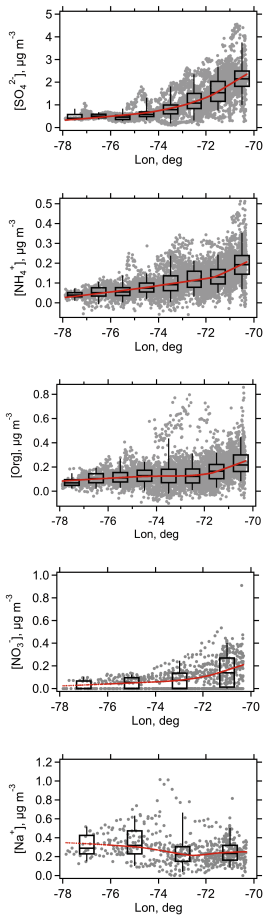

Fig. 4. Composite longitudinal dependence of below cloud (BC) aerosol concentrations determined on the G-1 for the entire VOCALS mission. Box plots (black) and LOWESS fits (red) are overlaid on individual data points (grey).

ACPD
13, 26043–26115, 2013

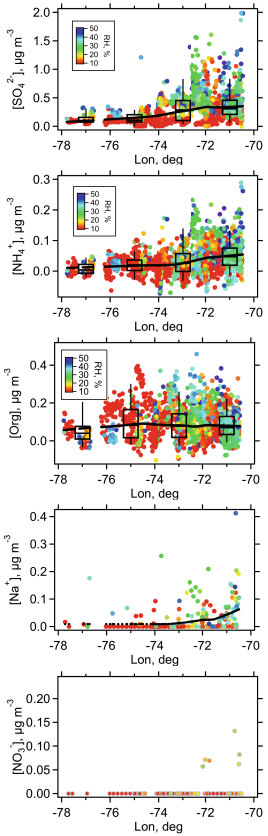

Fig. 5. Composite longitudinal distributions of aerosol concentrations of above cloud (AC) SO_4^{2-}, NH_4^+, Org, Na^+, and NO_3^- measured on the G-1 for the entire mission. Data are color coded to RH; solid black line represents LOWESS smooth. Box plots are for two-degree binned data.

ACPD
13, 26043–26115, 2013

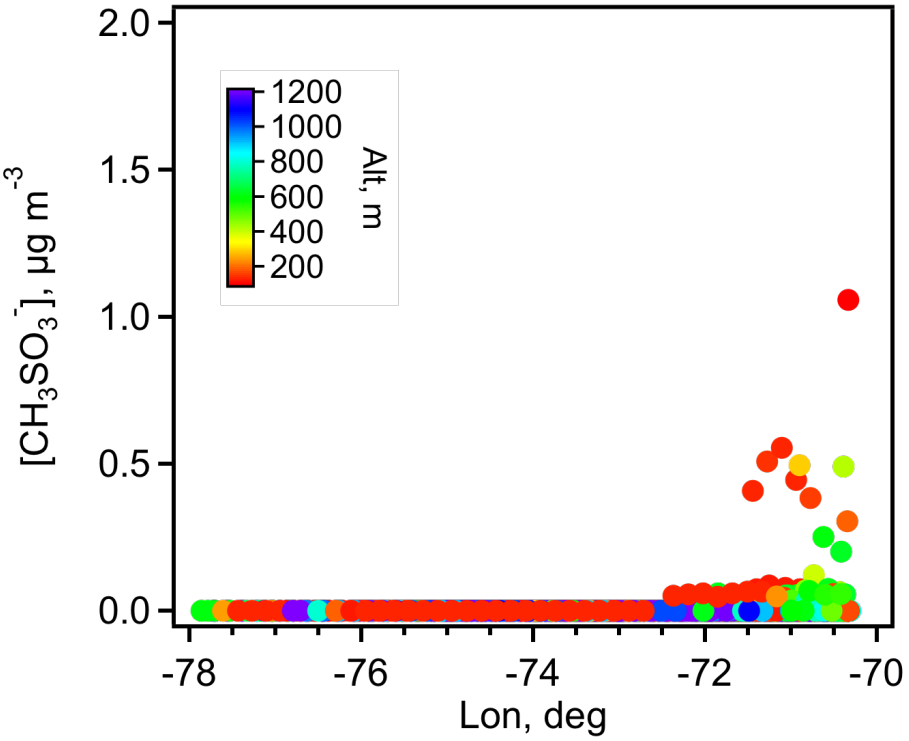

Fig. 6. Longitudinal dependence of aerosol MSA determined using the PILS-IC technique.

ACPD
13, 26043–26115, 2013

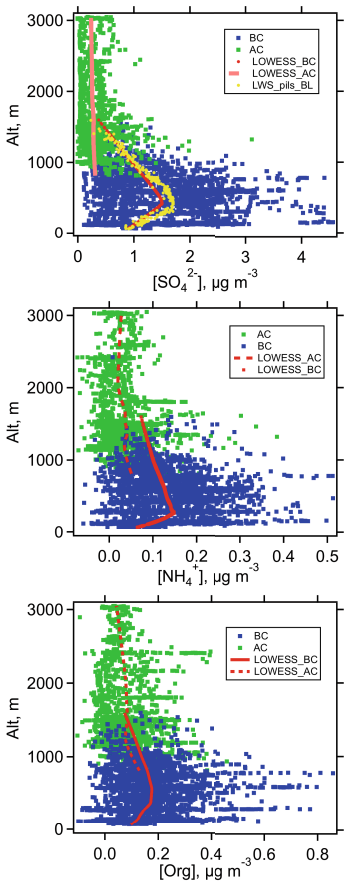

Fig. 7. Composite vertical distributions of the concentrations of SO_4^{2-}, NH_4^+, and Org for the entire G-1 mission. Continuous lines (dash as well as solid) represent LOWESS fits.

ACPD
13, 26043–26115, 2013

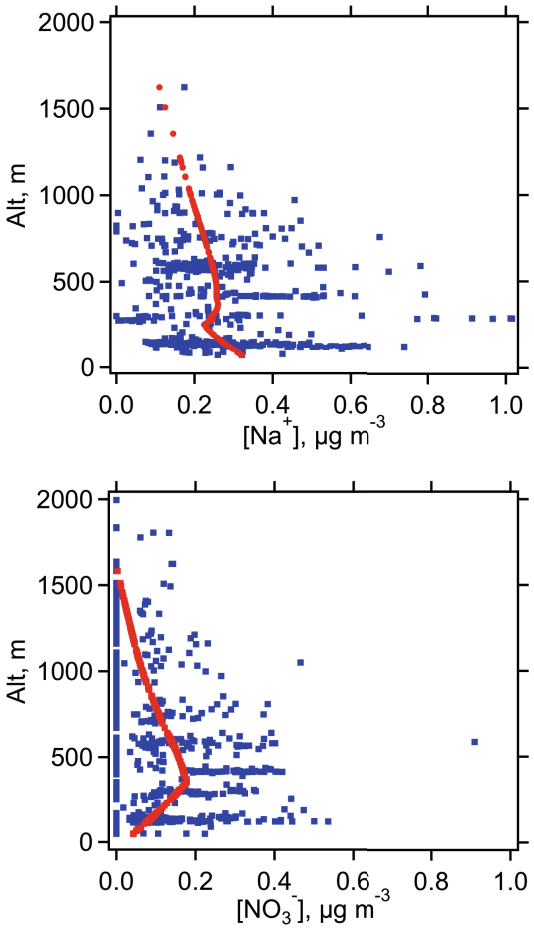

Fig. 8. Composite vertical distributions of below cloud (BC) aerosol Na^+ and NO_3^- concentrations. Red lines represent LOWESS fits.

ACPD
13, 26043–26115, 2013

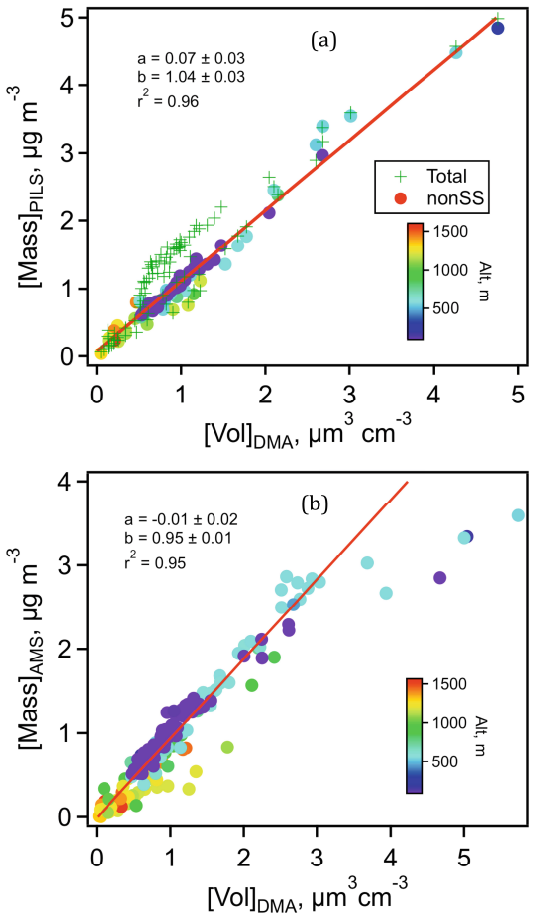

Fig. 9. Comparison of aerosol mass concentrations determined using the PILS and the AMS with the aerosol volume concentrations calculated from DMA size distributions. Solid lines are least squares best fits.

ACPD
13, 26043–26115, 2013

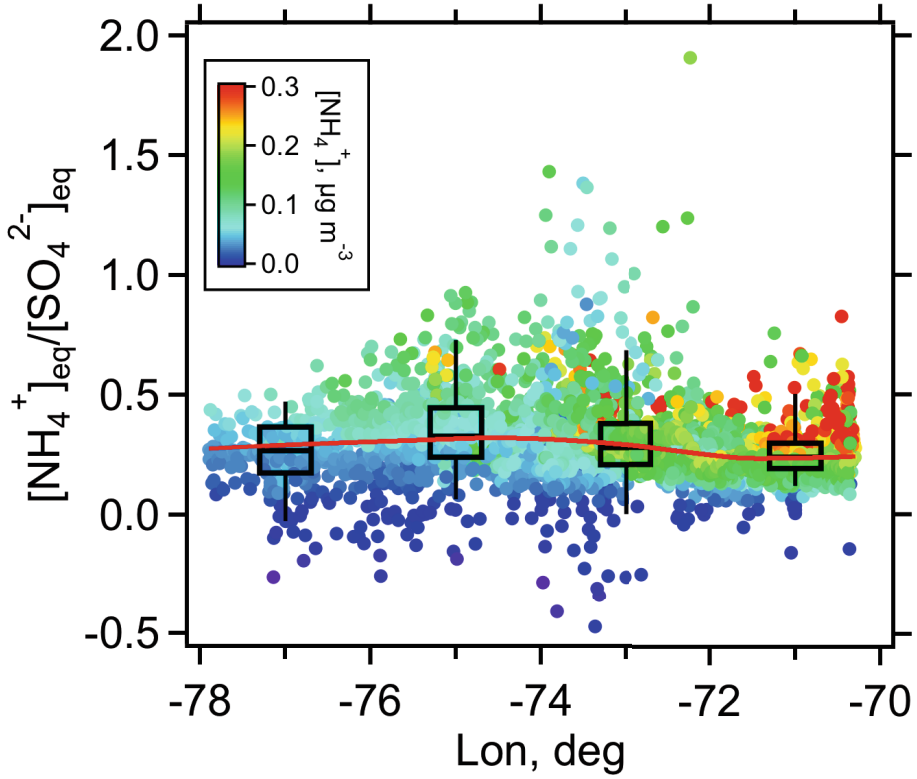

Fig. 10. Longitudinal dependence of the below cloud (BC) aerosol NH_4^+ to SO_4^{2-} equivalence concentration ratio. The red solid trace represents the LOWESS fit, and the box plots summarize the data in four longitude bins, i.e., −70° to −72°, −72° to −74°, −74° to −76°, and −76° to −78°.

ACPD
13, 26043–26115, 2013

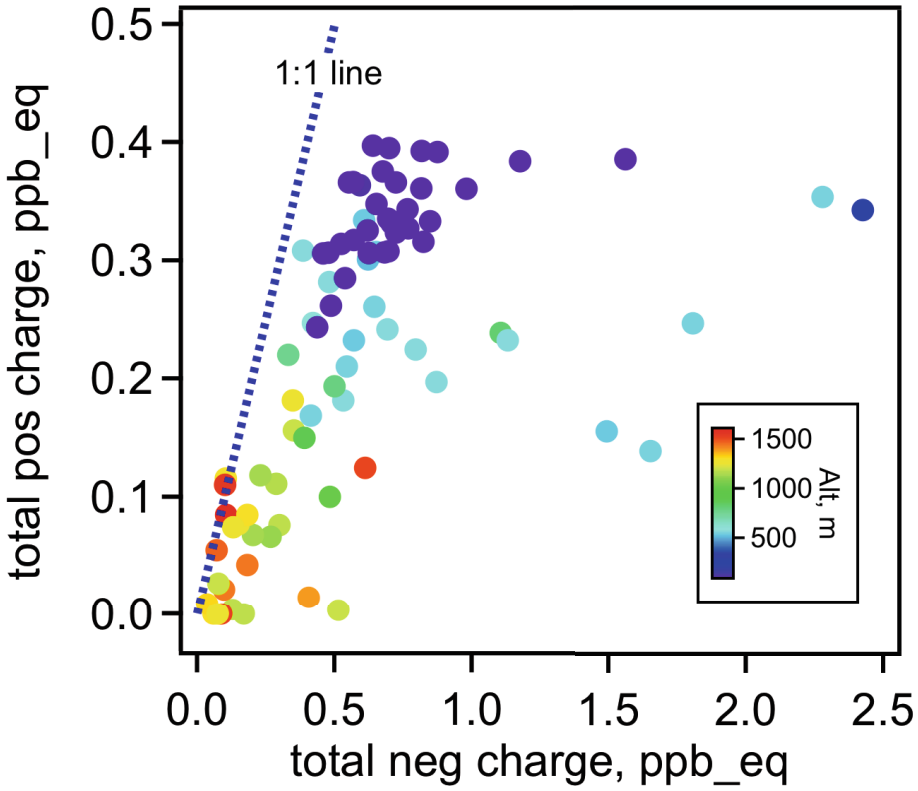

Fig. 11. Charge balance of aerosol components determined using the PILS-IC on 28 October 2008. The units are in parts-per-billion (ppb) multiplied by charge equivalence. Positive ions were dominated by Na^+ and NH_4^+; negative by Cl^-, NO_3^-, and SO_4^{2-}.

ACPD
13, 26043–26115, 2013

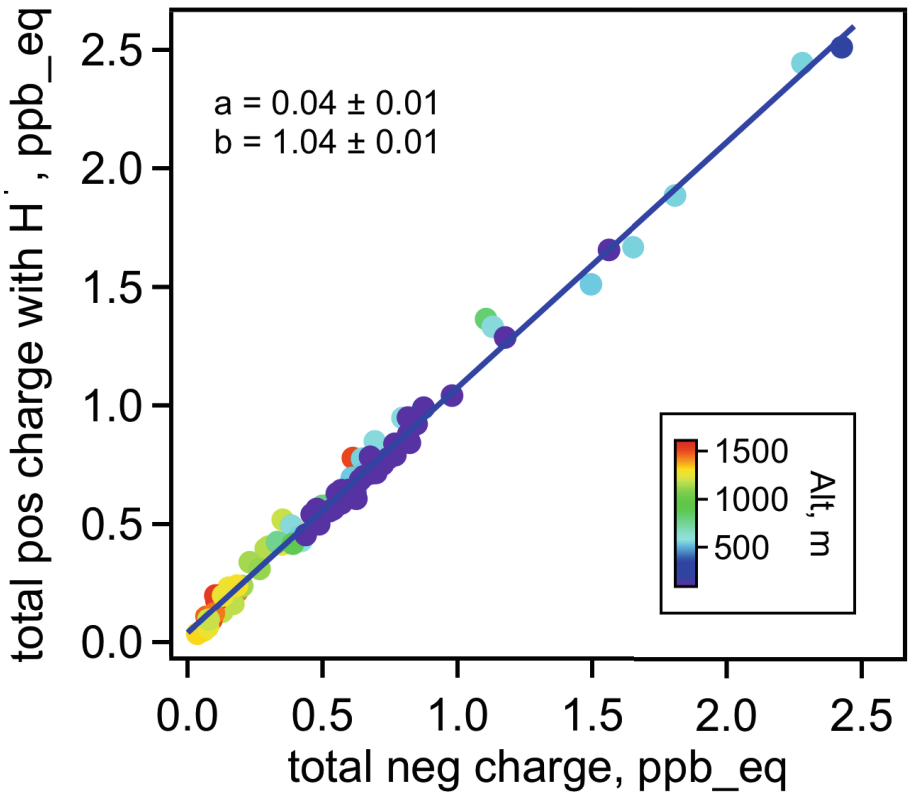

Fig. 12. Same as Fig. 11 except that the total positive charges now include H^+ as the missing cation associated with nss-SO_4^{2-}. The straight line represents the least square fit of the data with the values of the intercept, **(a)**, and slope, **(b)**.

ACPD
13, 26043–26115, 2013

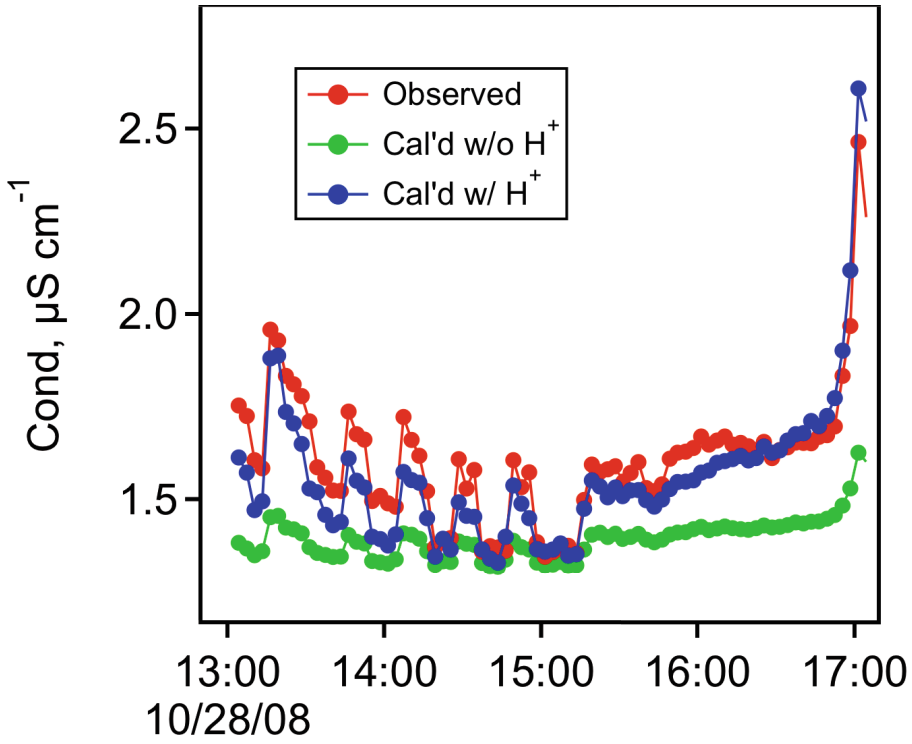

Fig. 13. Comparison of the observed and calculated conductivities of the liquefied aerosol samples collected by the PILS on the 28 October 2008 flight.

ACPD
13, 26043–26115, 2013

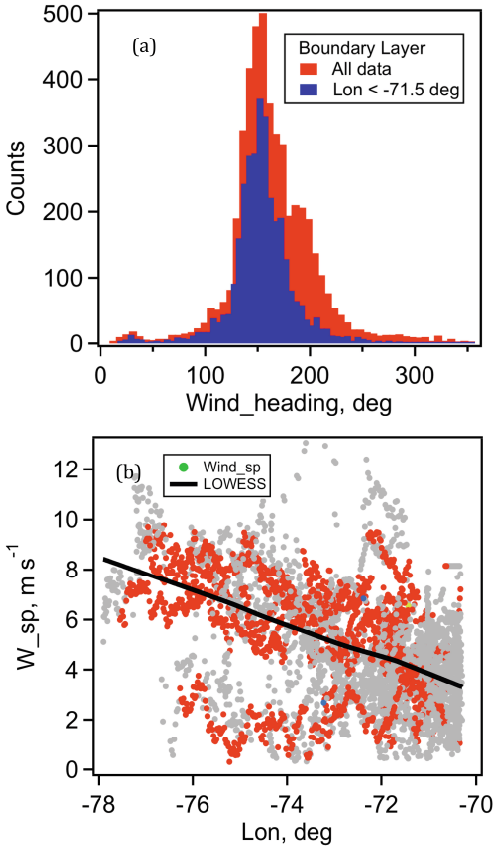

Fig. 14. (a) Histogram of MBL wind directions measured on the G-1 during VOCALS showing a consistent southerly near the coast that shifted slightly towards the NNW (155°) off shore. **(b)** Wind speed dependence on longitude where the black line represents the LOWESS fits, and the data points in red correspond to altitude less than 150 m.

ACPD
13, 26043–26115, 2013

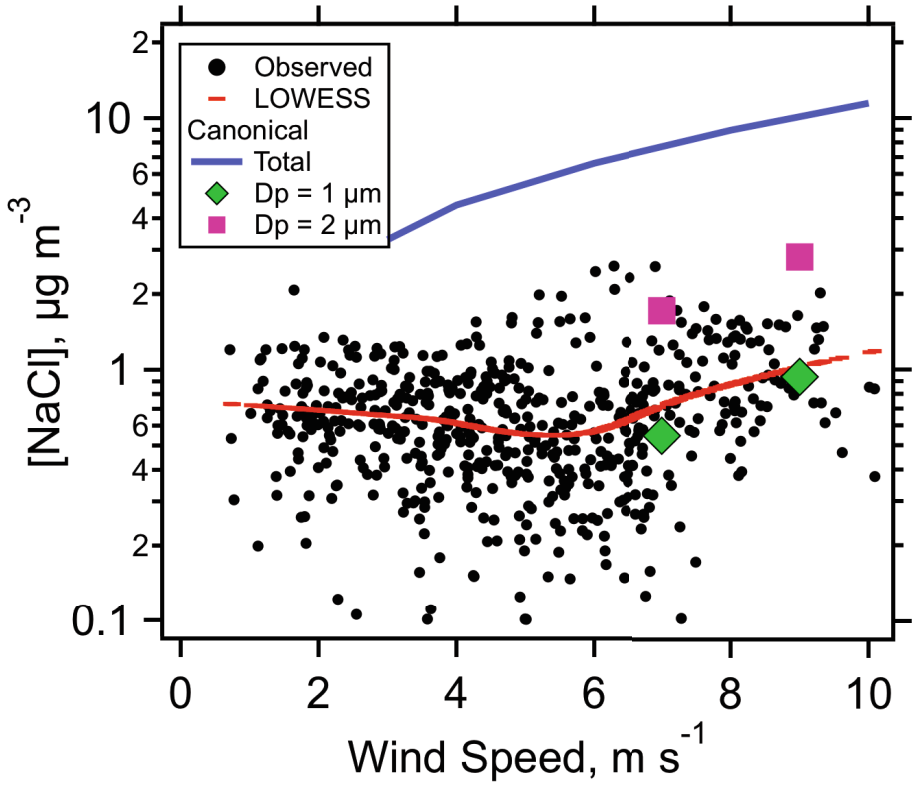

Fig. 15. Wind speed dependence of MBL SSA mass concentration (as NaCl) determined on the G-1 during VOCALS. The solid red line represents the LOWESS fit of the observed NaCl concentrations. The solid blue line represents empirical relationship between the total dry mass of SSA (scaled to NaCl) and the wind velocity at 10 m above sea surface (Fig. 17 in Lewis and Schwartz, 2004). The two sets of symbols in green and magenta represent the calculated concentrations with a 1 µm and 2 µm upper size cut, respectively.

ACPD
13, 26043–26115, 2013

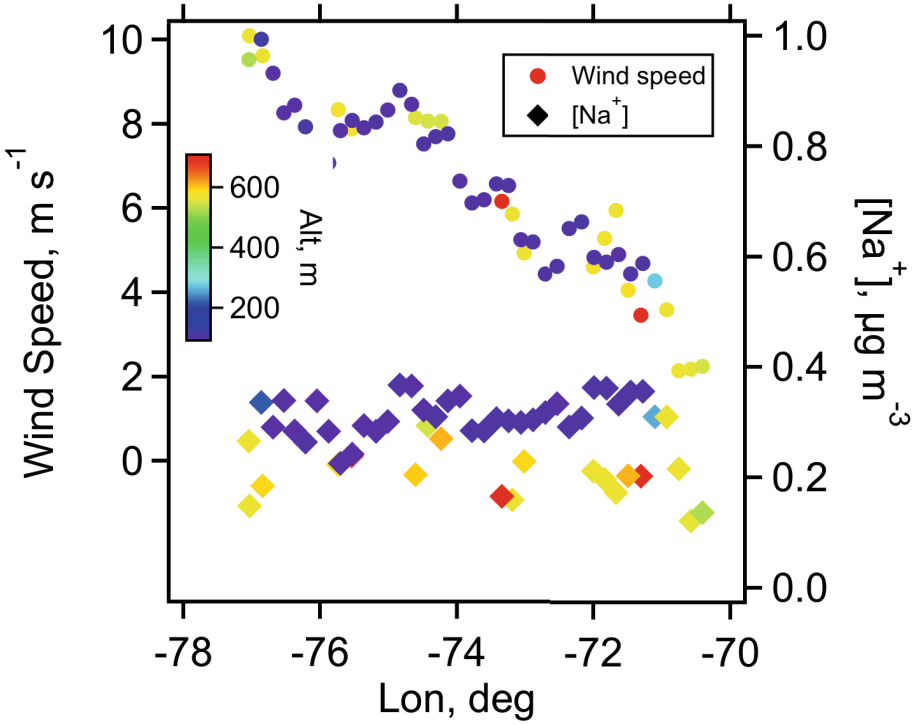

Fig. 16. Longitudinal variations of wind speed and SSA concentrations represented by Na^+ measured on 28 October 2008.

ACPD
13, 26043–26115, 2013

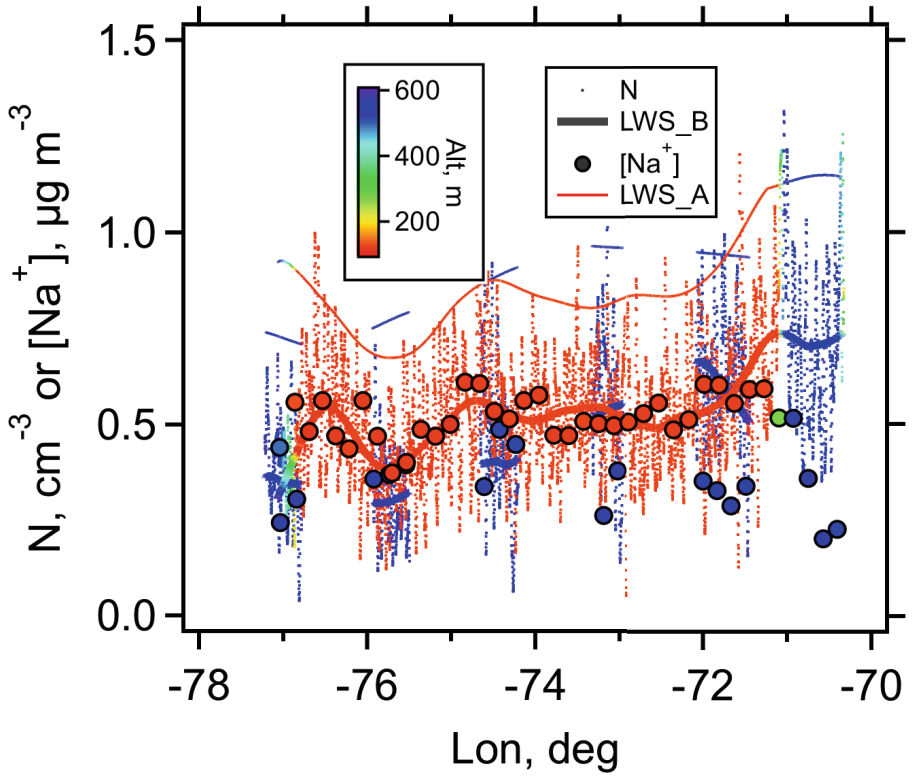

Fig. 17. Altitude dependence of below cloud (BC) [Na^+] and particle number concentrations between D_p = 0.5 µm and 3.0 µm measured using PCASP's on 28 October 2008. Total number concentration: dots (1 s data: inboard PCASP only; outboard PCASP data not shown); Na^+ concentration: solid circles; LOWESS fits to $N_{0.5-3}$: thin solid lines (outboard PCASP, A), thick solid lines (inboard PCASP, B). All color-coded to altitude: blue ~ 600 m and red ~ 100 m.

ACPD
13, 26043–26115, 2013

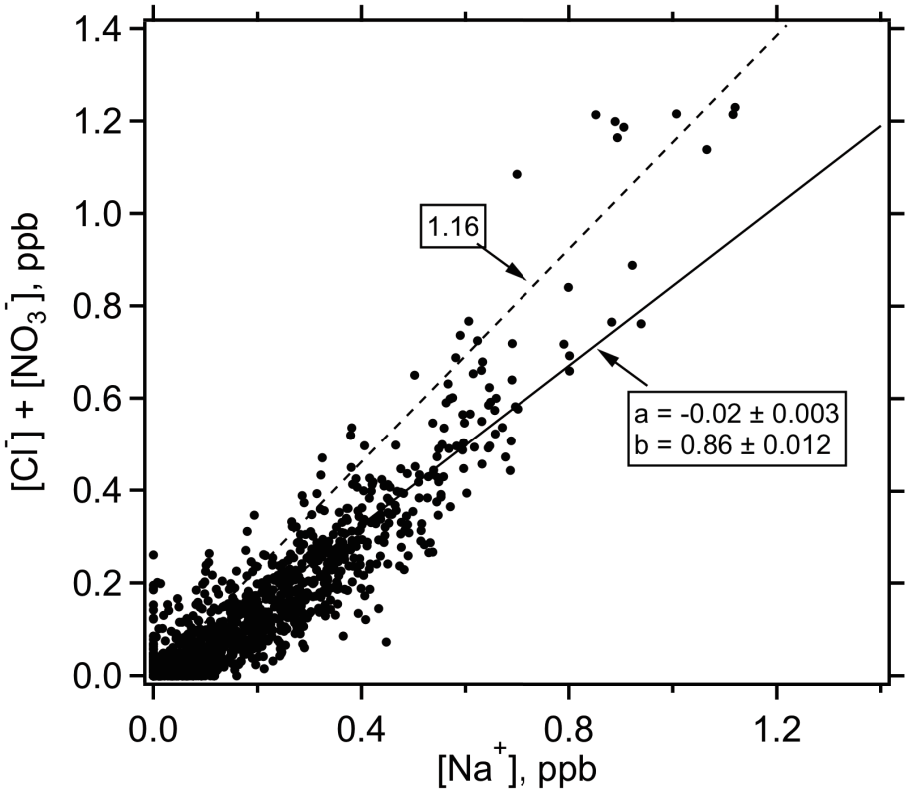

Fig. 18. Relationship between concentrations of aerosol Cl^- and Na^+ with NO_3^- included to account for the displaced Cl^- due to SSA acidification by H_2SO_4. The dash line represents the sea-water Cl^- to Na^+ ratio of 1.16, and the solid line a least square fit of the data whose intercept and slope are indicated.

ACPD
13, 26043–26115, 2013

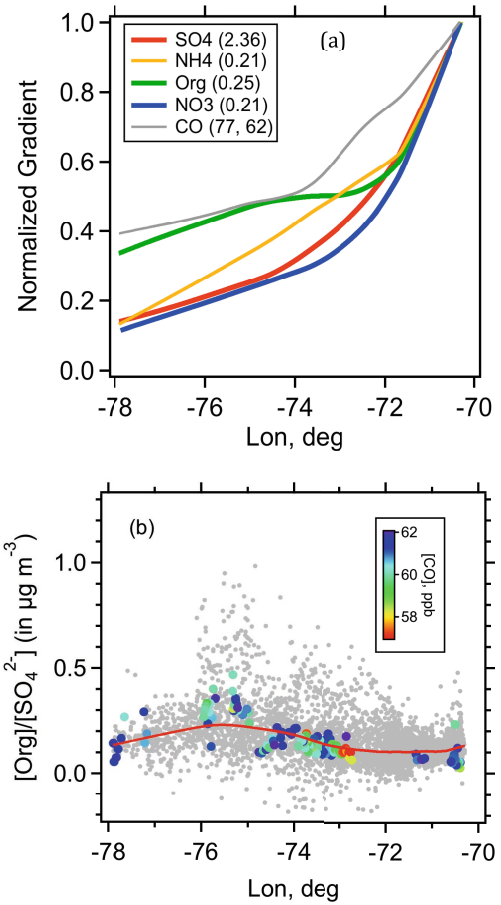

Fig. 19. (a) Normalized composite longitudinal distributions of below-cloud SO_4^{2-}, NH_4^+, Org, NO_3^-, and CO. **(b)** Dependence of [Org]/[SO_4^{2-}] ratio on longitude, where the solid red line represents the LOWESS fit of the data.

ACPD
13, 26043–26115, 2013

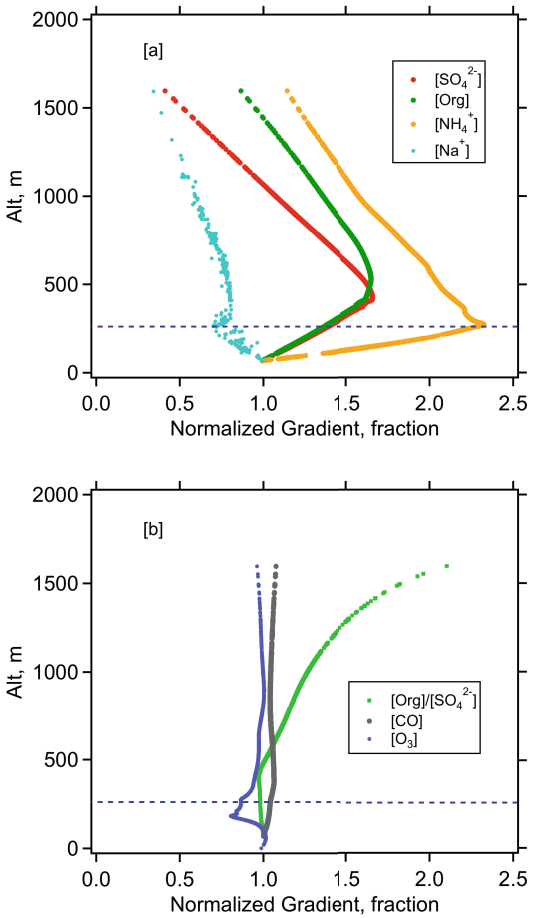

Fig. 20. Normalized vertical distribution profiles of **(a)** BC aerosol SO_4^{2-}, NH_4^+, Org, and Na^+; **(b)** BC O_3 and CO as well the $[Org]/[SO_4^{2-}]$ ratio.

ACPD
13, 26043–26115, 2013

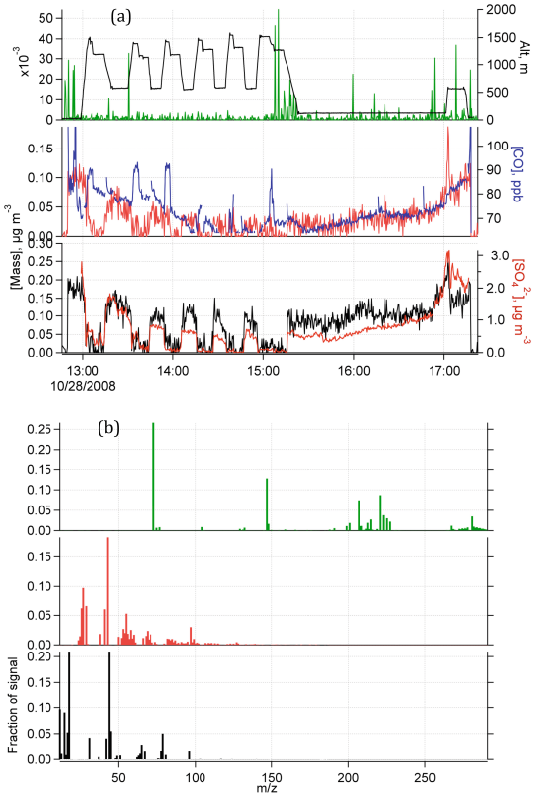

Fig. 21. PMF analysis results of 28 October 2008 data with $p = 3$ and $F_{peak} = 0.4$. **(a)** Time series of factors 1, 2, and 3 representing mass concentrations (left ordinates) shown from bottom to top in black, blue, and green, respectively. Overlaid on time series of factors 1, 2, and 3 are $[SO_4^{2-}]$, [CO], and altitude (right ordinates), respectively. **(b)** Mass spectrum profiles of factors 1, 2, and 3 with the same color designation.

ACPD
13, 26043–26115, 2013

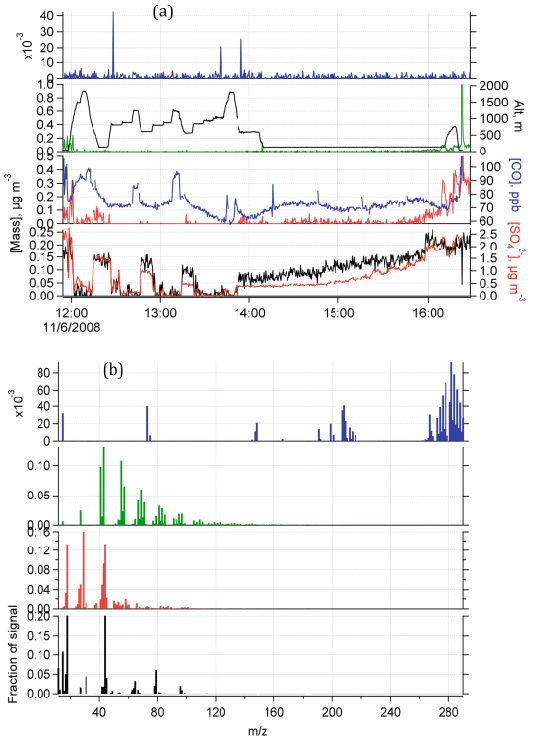

Fig. 22. PMF analysis results of 6 November 2008 data with $p = 4$ and $F_{peak} = 0.4$. **(a)** Time series of factors 1, 2, 3, and 4 representing mass concentrations shown in black, red, and green, respectively. Overlaid on time series of factors 1, 2, and 3 are $[SO_4^{2-}]$, [CO], and flight altitude, respectively. **(b)** Mass spectrum profiles of the 4 factors with the same color designations.

ACPD
13, 26043–26115, 2013

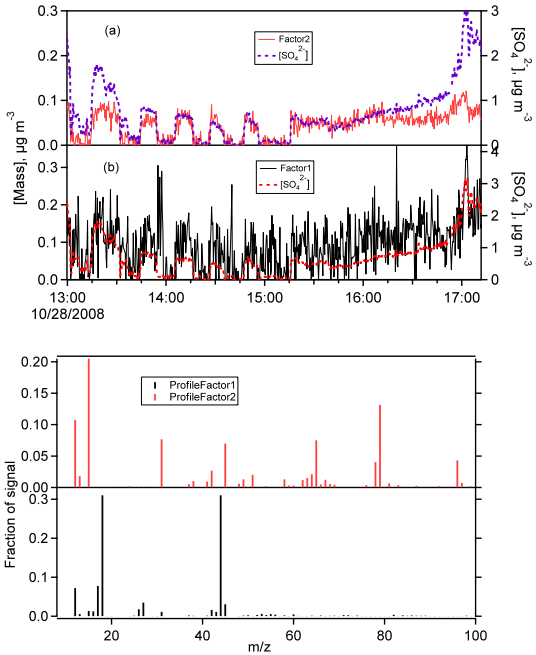

Fig. 23. PMF analysis results of 28 October 2008 data with $p = 5$ and $F_{peak} = 0$: with only factors 1 and 2 displayed.

ACPD
13, 26043–26115, 2013

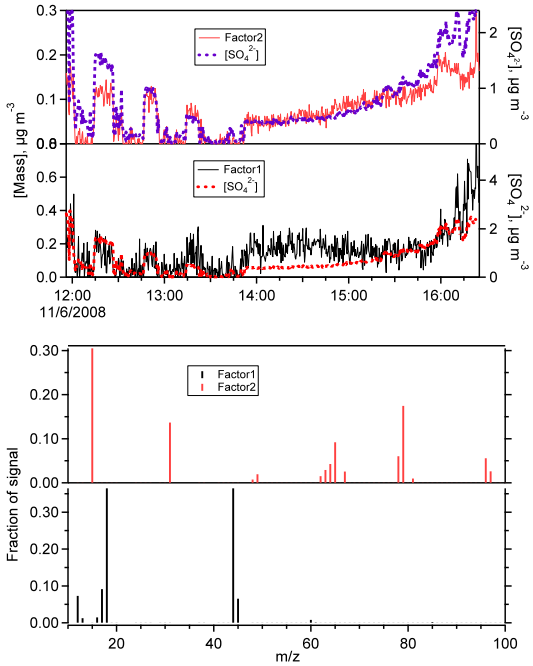

Fig. 24. PMF analysis results of 6 November 2008 data with $p = 6$ and $F_{peak} = 0.6$: with only factors 1 and 2 displayed.

ACPD
13, 26043–26115, 2013

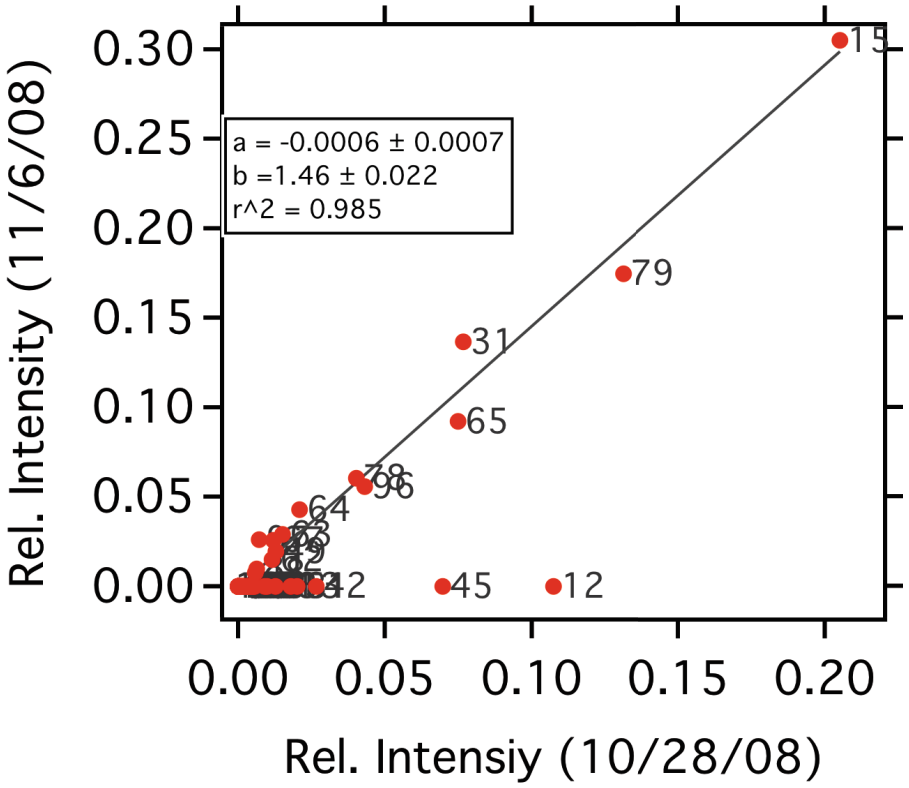

Fig. 25. Correlation of MSA mass spectrum fragments obtained on the 28 October 2008 and 6 November 2008 flights.

ACPD
13, 26043–26115, 2013

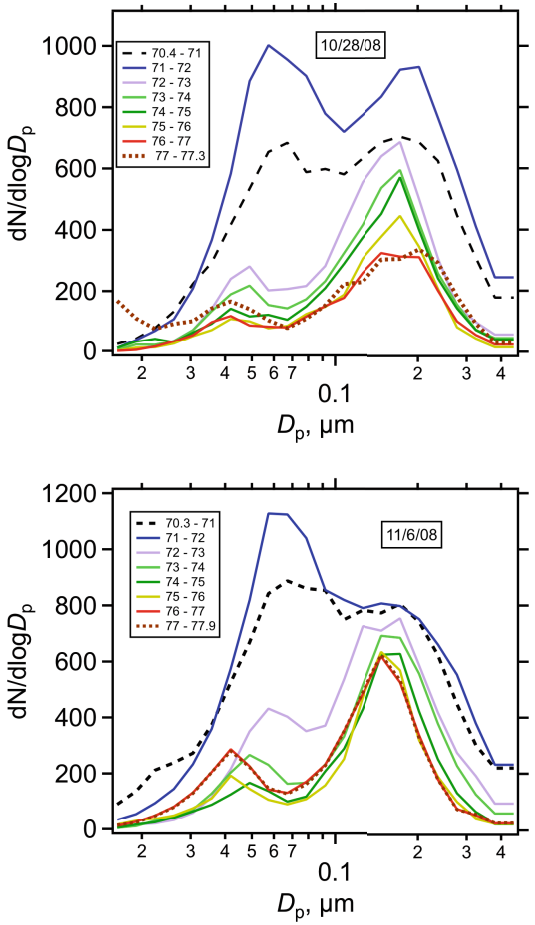

Fig. 26. MBL aerosol particle size distributions during return legs on 28 October 2008 and 6 November 2008 as a function of longitude with data binned into 1-degree intervals.

ACPD
13, 26043–26115, 2013